Master Thesis

Recommendation system for scientific tools and workflows

Anup Kumar

University of Freiburg

Faculty of Engineering

Department of Computer Science

Bioinformatics Group, Freiburg

July 09, 2018

Thesis period

08. 01. 2018 – 09. 07. 2018

Examiners

Prof. Dr. Rolf Backofen and Prof. Dr. Wolfgang Hess

Adviser

Dr. Björn Grüning

Declaration

I hereby declare, that I am the sole author and composer of my thesis and that no other sources or learning aids, other than those listed, have been used. Furthermore, I declare that I have acknowledged the work of others by providing detailed references of said work.

I hereby also declare, that my Thesis has not been prepared for another examination or assignment, either wholly or excerpts thereof.

_____   _____
Place, Date   Signature

Dedicated to my mom and dad

Acknowledgement

Zusammenfassung

Die Arbeit erforscht zwei Konzepte, um ein Empfehlungssystem für Galaxy's wissenschaftliche Datenverarbeitungs-Tools und Workflows zu entwickeln. Die Konzepte werden in dieser Arbeit separat behandelt und beinhalten das Auffinden von Ähnlichkeiten in Tools und die Vorhersage nachfolgender Tools in Workflows. Der erste Teil untersucht die Methode zum Auffinden von Ähnlichkeiten bei Tools, einschließlich der Existenz ähnlicher Tools für ein jeweiliges Tool in einem Tool-Bündel. Darüber hinaus wird die Ähnlichkeit zwischen Tools quantifiziert durch das Zuweisen eines Ähnlichkeitswertes zu jedem Tool-Paar. Die Ähnlichkeit von Tools wird durch Ansätze aus der natürlichen Sprachverarbeitung und Optimierung berechnet. Für diese Aufgabe wurden über 1.000 Tools verwendet. Die Daten der Tools wurden aus verschiedenen Eigenschaften, einschließlich Name, Beschreibung, Eingabe- und Ausgabe-Datentypen und Hilfstexten gesammelt. Der zweite Teil der Arbeit entwirft ein Vorhersage-System, welches die möglichen nächsten Tools in Workflows darlegt. Diese wissenschaftlichen Workflows sind komplex und werden mit mehr als erstellt 4.000 Tools in der Bioinformatik. Die Kenntnis möglicher nächster Tools kann es weniger erfahrenen Galaxy-Benutzern leichter machen, Workflows zu erstellen. Außerdem kann die zur Erstellung eines Workflows benötigte Zeitdauer verkürzt werden. Die einzelnen, aus Workflows (gerichtete azyklische Diagramme) entnommenen Wege (Tool-Sequenzen) werden in periodische neuronale Netzwerke eingebracht, um die Semantik von Tool-Verbindungen zu ermitteln. Aus der Erfahrung von höheren, in diesen Tool-Verbindungen vorherrschenden Abhängigkeiten, werden die Vorhersagen gemacht. Um das Vorhersage-Modell in Erfahrung zu bringen wurden über 167.000 Pfade verwendet.

Abstract

The thesis enquires into two concepts to develop a recommendation system for the Galaxy's scientific data-processing tools and workflows. The concepts incorporate finding similarity in tools and predicting next tools in workflows and are dealt with separately in the thesis. The first part explores a way to find similarity in tools. It implies which similar tools exist for each tool within a cluster of tools. In addition, it quantifies the similarity among tools by assigning a similarity score for each pair of tools. The similarity in tools is computed using the approaches from natural language processing and optimisation. Over $1,000$ tools have been used for this task. The metadata of tools is gathered from multiple attributes including name, description, input and output data types and help text. The second part formulates a prediction system to display the next possible tools in scientific workflows. These scientific workflows are complex and are created using more than $4,000$ tools in the bioinformatics field. The knowledge of the next possible tools can make it easier for the less experienced Galaxy users to create them. Moreover, it can curtail the amount of time taken to create a workflow. The unique paths (tools sequences) extracted from the workflows are fed to the recurrent neural networks to learn the semantics of tools connections. The predictions are made by learning higher-order dependencies prevalent in these tools connections. More than $167,000$ paths have been utilised to learn the predictive model.

Contents

List of Figures

List of Tables

Part I.

Find similar scientific tools

1. Introduction

1.1. Galaxy

Galaxy is an open-source biological data processing and research platform [1]. It supports numerous types of data formats like *fasta*, *fastaq*, *gff*, *pdb* and many more[1] and they are extensively used for data processing. It offers scientific tools and workflows to transform these datasets (figure 1). Each tool has an exclusive way to process datasets. A couple of examples of data processing are to merge two compatible datasets to make one and to reverse complement a sequence of nucleotides[2].
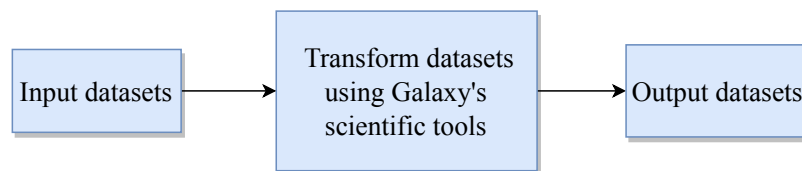
Figure 1.: Dataset transformation: The image shows a general flow of data transformation using the Galaxy's scientific tools.

Tools are classified into multiple categories based on their functions and types. For example, the tools which manipulate text, like replacing texts and selecting lines of a dataset, are grouped together under *text manipulation* category. Similarly, there are various tool categories like *imaging*, *convert formats*, *genome annotation* and many others[3]. These tools are the building blocks of a workflow. A workflow is data processing pipeline where a set of tools are joined one after another. The connected tools in the workflow should be compatible with each other. It means that the output file types of one tool should be present in the input file types of the next tool. An example of a workflow is *variantcalling-freebayes*. It is used for the detection of variants (specifically single and multiple nucleotide polymorphisms and insertions and deletions) following a bayesian approach.

---

[1] https://galaxyproject.org/learn/datatypes/
[2] https://usegalaxy.eu/?tool_id=MAF_Reverse_Complement_1&version=1.0.1
[3] https://toolshed.g2.bx.psu.edu/repository

1.2. Scientific tools

A tool entails a specific function. It consumes a dataset, brings about some transformations and produces an output dataset which is fed to other tools. For example, *trimmomatic* tool trims a *fastq* file and produces a *fastqsanger* file which is used as an input file to a different tool like *fastqc*. A tool has multiple attributes which include its input and output file types, name, description, help text and many more[4]. These attributes constitute the metadata of a tool. The metadata shows that some tools have similar functions while some share similarities in their input and output file types. For example, a tool *hicexplorer hicpca*[5] has an output type named *bigwig*. A tool which also has *bigwig* as its input and/or output type, there is some similarity between these tools as they do a transformation on similar file type. Similar tools can also be found by analysing other attributes like name or description.
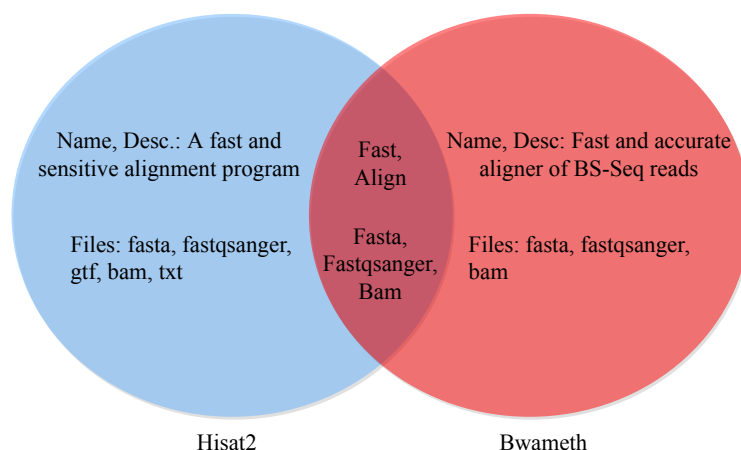
Figure 2.: Common features of two tools: The venn diagram shows common features of two tools - *hisat2* and *bwameth*. Based on their common features, shown in the middle of the venn diagram, similarity between them is assessed.

Figure 2 shows two tools - *hisat2* and *bwameth*. Their respective metadata is collected from their input and output file types and name and description attributes. Both of them share common file types (*fasta, fasaqsanger, bam*). Moreover, they share a similar function of aligning. By extrapolating this method of finding similar features among tools, a set of similar tools for each tool can be created.

---

[4]https://docs.galaxyproject.org/en/master/dev/schema.html

[5]https://usegalaxy.eu/?tool_id=toolshed.g2.bx.psu.edu/repos/bgruening/
hicexplorer_hicpca/hicexplorer_hicpca/2.1.0&version=2.1.0

1.3. Motivation

The Galaxy has thousands of tools with a diverse set of functions. New tools keep getting added to the existing set of tools. For a user, it is hard to keep knowledge about so many existing tools. In addition, it is important to make users aware of the presence of the newly added tools. They may be similar to some of the existing tools. A set of similar tools for a tool would give more options to the users for their data processing.
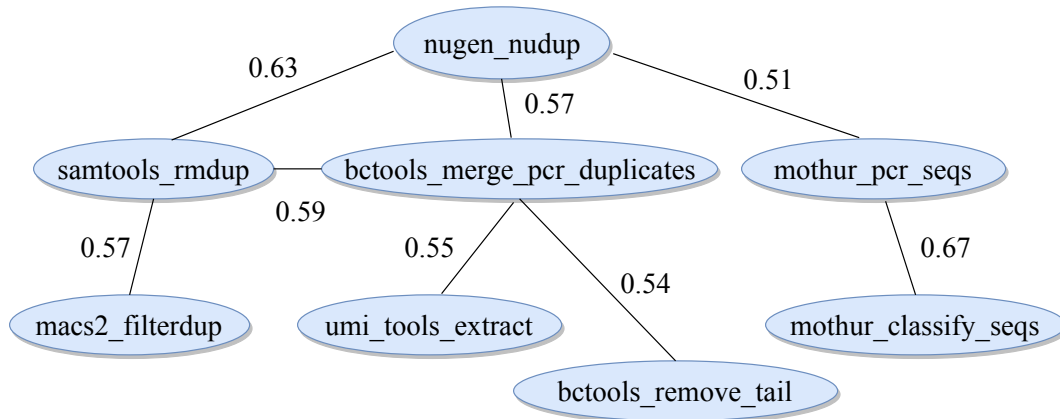
Figure 3.: Similarity graph of tools: In the graph, the nodes are represented by tools and the edges show similarity scores for each pair of tools. Higher the similarity score, more similar a pair of tools are.

To elaborate more, a tool *nugen nudup*[6] (figure 3) is taken. It is used to find and remove PCR duplicates. A few of its similar tools are found. The similar tools like *samtools rmdup* and *bctools merge PCR duplicates* also have a similar function. Each tool has a set of similar tools and together they make a graph of the related tools. This similarity graph shows *connectedness* among tools and can help a user to find multiple ways to process data by replacing a tool with its similar tool. Figure 3 shows a small example of the similarity graph.

---

[6]https://toolshed.g2.bx.psu.edu/repository?repository_id=4f614394b93677e3

2. Approach

This section gives a comprehensive description of the approach to compute similarity among tools. It involves a sequence of steps. The metadata of tools is extracted from the *github's* tool repositories. It is cleaned to get a set of words for each tool which uniquely identifies it. This set is used to create a fixed-length vector for each tool. The words from all the tools are merged to create a collection. Its size gives the size of the vector. Each word from the collection has a position in the vector. In the vector of a tool, the positions of the respective words (words from the tool's set) contain the frequency of their occurrence. The positions of those words not present in the set for a tool contain zero. These vectors are used to compute similarity scores for each pair of tools using similarity measures. The similarity scores of each tool with all the other tools create a similarity matrix. A similarity matrix is computed for each attribute. These similarity matrices are combined by optimisation to get a weighted average similarity matrix (figure 4). All the steps to compute similarity among tools are explained in further sections.

2.1. Extract tools data

The Galaxy's scientific tools are stored at *github* across multiple repositories. One such repository is *Galaxy tools maintained by IUC*[1]. A tool is defined in an *extensible markup language (XML)* file which can be parsed efficiently to gather the metadata from multiple attributes. The *XML* files of tools start with a *tool* tag.

2.1.1. Attributes

A tool has multiple attributes which include input and output file types, help text, name, description, citations and many more[2]. But, not all of these attributes are

---

[1] https://github.com/galaxyproject/tools-iuc
[2] https://docs.galaxyproject.org/en/master/dev/schema.html
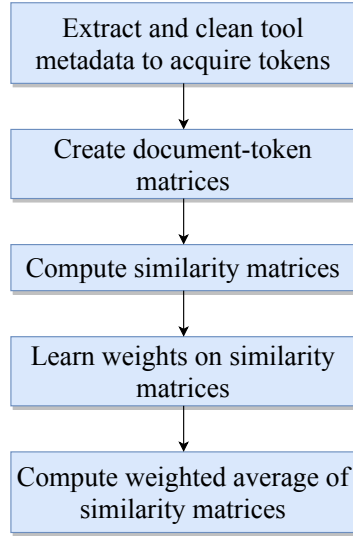
Figure 4.: Sequence of steps to find similar tools: The flowchart shows a series of steps to establish similarity among tools using the approaches from natural language processing to compute similarity matrices and optimisation to compute a weighted average of the similarity matrices.

significant in identifying a tool. Therefore, only the following attributes are considered to collect the metadata of tools:

- Input file types

- Output file types

- Name

- Description

- Help text

Moreover, the input and output file types are combined by taking a union set to create one attribute as together they contain information about file types of a tool. A similar combination is done for the name and description attributes as well. These combined attributes give a complete metadata of a tool's file types (input and output types) and its functionality (name and description). Further, the help text attribute is also included in the metadata. This attribute contains more information compared to the previous two combined attributes. Apart from being larger in size, it is noisy as well. It gives a detailed information about the functions of a tool and the format of

its input data[3]. Much of the information contained by this attribute is not important to clearly distinguish a tool. Therefore, only the first few lines of text from this attribute are considered which illustrate the core functionality of tools. The rest of the information is discarded.

2.1.2. Gather useful metadata

Remove duplicates and stop-words

The metadata of tools collected from multiple attributes is raw. It contains lots of noisy and duplicate items which do not add value. These items should be removed from the metadata to get tokens which are unique and useful. For example, a tool *bamleftalign* has *bam* and *fasta* as input files and *bam* as an output file. While combining these file types to make a set of file types for a tool, the duplicates are discarded. Hence, the *bam* and *fasta* together make a set of file types for the tool. This set does not maintain any order of the file types. The attributes like the name and description and help text contain sentences (complete or partially complete) in the English language. Therefore, to process these, strategies from natural language processing[4] are needed. A sentence contains many words and can have many different parts of speech. The parts of speech include a subject, object, preposition, interjection, verb, adjective, adverb, article and many more[5]. Only those words are taken out from the sentences which categorise a tool uniquely. For example, the tool *tophat* has a name and description which is read as *tophat for illumina find splice junctions using RNA-seq data*. The words like *for*, *using* and *data* cannot distinguish the tool as they can be present in the description of many other tools. These words are called stop-words[6] and are discarded. In addition, the numbers are also removed. All the remaining words are converted to the lower case.

Use stemming

After removing the duplicates and stop-words, the metadata becomes clean and contains words which can identify tools uniquely. Different forms of a word are used in sentences due to the rules of grammar. For example, a word *regress* has multiple

---

[3]https://planemo.readthedocs.io/en/latest/standards/docs/best_practices/tool_xml. html#help-tag
[4]https://www.ncbi.nlm.nih.gov/pmc/articles/PMC3168328/
[5]https://web.stanford.edu/~jurafsky/slp3/10.pdf
[6]https://www.ranks.nl/stopwords

forms like *regresses* or *regression* or *regressed*. All these forms share the same root and point towards the same concept. Therefore, it is beneficial to converge all the different forms of a word to one basic form. This process is called stemming[7]. The *NLTK*[8] package is used for stemming. It reduces the size of metadata and keeps the meaning of a word same across multiple forms. After stemming, the words would be called tokens. Figure 5 shows a distribution of tokens in the metadata for all the three attributes of tools. These tokens are used for computing similarity among tools. The help text attribute contains more tokens than input and output file types and name and description attributes.
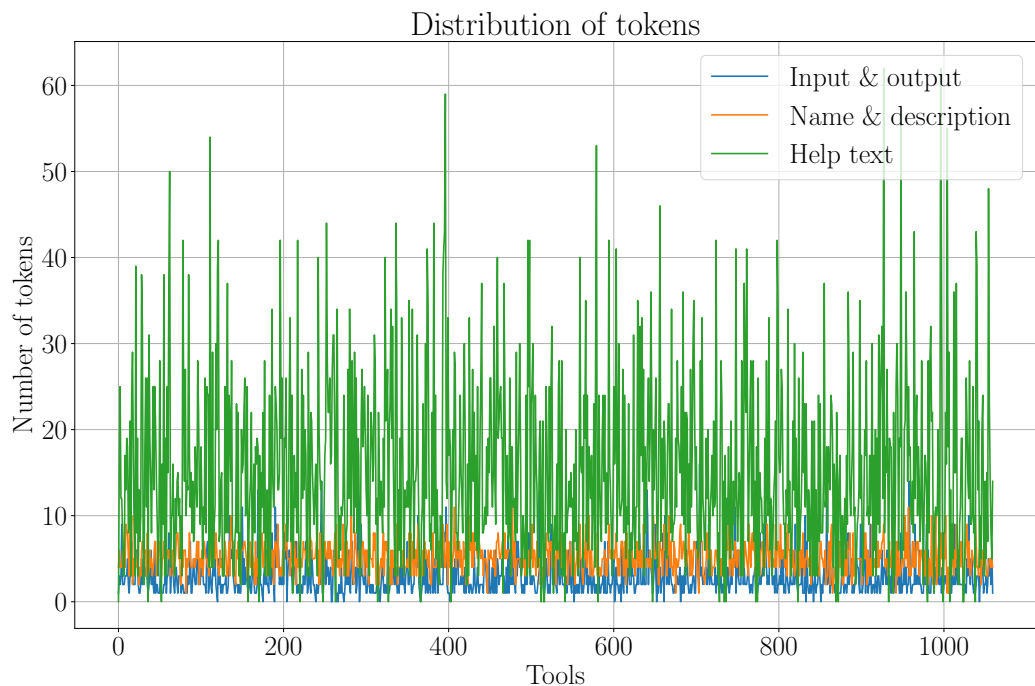
Figure 5.: Distribution of tokens: The plot shows a distribution of the number of tokens for input and output file types, name and description and help text attributes of tools.

---

[7]https://nlp.stanford.edu/IR-book/html/htmledition/stemming-and-lemmatization-1.html

[8]http://www.nltk.org/
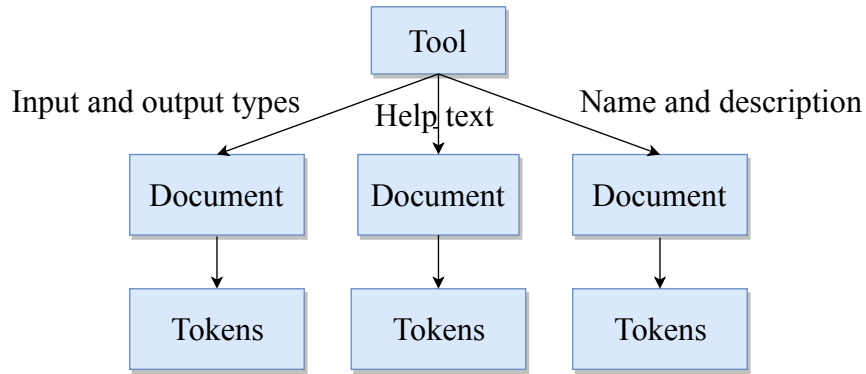
Figure 6.: Relationship between a tool, its documents and their tokens:
The image shows that a tool has three documents corresponding to each
attribute and each document contains tokens. The documents are equal
to the number of tools for each attribute. The number of tokens in each
document varies.

Learn relevance for tokens

After stemming the words from metadata, meaningful sets of tokens are collected
for input and output file types, name and description and help text. These sets are
called documents (figure 6). The tokens present in these documents do not carry
equal importance. Some tokens are more relevant to a document, but some are not.
An importance factor is computed for each token in a document. These factors
are arranged in a big, sparse document-token matrix. Each attribute has its own
document-token matrix. In these matrices, each row represents a document and each
column represents a token. To compute these importance factors, the *bestmatch25
(BM25)* [2] algorithm is used. The variables used in implementing this algorithm are
as follows:

- Token frequency[9] (tf)

- Document frequency (df) and inverted document frequency (idf)

- Average document length ($|D|_{avg}$)

- Number of documents (N)

- Size of a document ($|D|$)

---

[9]https://nlp.stanford.edu/IR-book/pdf/06vect.pdf

A token frequency (tf) gives the count of a token's occurrence in a document. If a token *regress* appears twice in a document, its tf is 2. It is a weight given to the token. Inverted document frequency (idf) for a token is defined as:

$$idf = \log \frac{N}{df} \qquad (1)$$

where df is the count of documents in which the token is present and N is the total number of documents. If a document is randomly sampled from a set of documents, the probability of the token to be present in this document is $p_i = \frac{df}{N}$. From information theory [3], the information contained by this event is computed by $-\log p_i$. The idf is higher when a token appears only in a few documents. It means that the token is a good candidate for representing that document. The tokens which appear in many documents are not good representatives of those documents. The average document length ($|D|_{avg}$) is the average number tokens computed over all the documents. The size of a document ($|D|$) is the count of all the tokens for that document. *BM25* score of a token is calculated using the following equations:

$$\alpha = (1 - b) + \frac{b \cdot |D|}{|D|_{avg}} \qquad (2)$$

$$tf^* = tf \cdot \frac{k + 1}{k \cdot \alpha + tf} \qquad (3)$$

$$BM25_{score} = tf^* \cdot idf \qquad (4)$$

where k and b are the hyperparameters of the *BM25* and their ideal values should be found according to the data. k is always a positive number. When k is zero, the $BM25$ score for a token is defined only by its idf ($tf^* = 1$). When k is a large number, the $BM25$ score is computed using the raw term frequency ($tf^* = tf$). b is a real number between zero and one ($0 \leq b \leq 1$). When b is zero, the document length is not normalised. It means that the fraction $\frac{|D|}{|D|_{avg}}$ is not accounted for computing the $BM25$ score. When b is one, this fraction is completely accounted for. In this case, when $|D| >> |D|_{avg}$ for any document, its tokens would get a lower $BM25$ score. For this work, the standard values of k and b (1.75 and 0.75 respectively) are used. Using equation 4, the $BM25$ score is computed for each token in all the documents. Table 1 shows the $BM25$ scores for four documents (rows) along with five tokens (columns). Following this approach, the document-token matrices are

computed for all the three attributes of tools. For input and output file types, the matrix will have only two values, one if a token is present for a document and zero if not. For other attributes, the $BM25$ scores are positive real numbers.

Document/token	regress	linear	gap	mapper	perform
LinearRegression	5.22	4.1	0.0	0.0	3.84
LogisticRegression	3.54	0.0	0.0	0.0	2.61
Tophat2	0.0	0.0	1.2	1.47	0.0
Hisat	0.0	0.0	0.0	0.0	0.0

Table 1.: A sparse document-token matrix: The table shows a matrix of documents arranged along the rows and tokens along the columns. Each value in the matrix is a $BM25$ score assigned to a token. The matrix is sparse because the total number of tokens (for all the documents) is larger than the number of tokens present for each document.

The document-token matrices are sparse. Each entry in these matrices is a $BM25$ score for each token. This representation is important to know which tokens are better representatives, but which are not for a document. They do not give any information about the co-occurrence of tokens in a document. A token is important for a document if the $BM25$ score is high but it does not give any information about its relation to the other tokens. The information about the co-occurrence of tokens in a document defines a concept hidden in that document. A concept in a document is formed by using the relation among a few tokens. To illustrate this idea, an example of three words, *New York City*, is considered. These three words mean little and point to different things if each word is considered separately. But, together they point towards a concept. The $BM25$ model lacks the ability to find the correlation among tokens. To learn hidden concepts within documents and find correlation among tokens, two approaches are explored:

- Latent semantic analysis[10]

- Paragraph vectors

Using these approaches, a multi-dimensional dense vector is learned for each document.

---

[10]http://lsa.colorado.edu/papers/dp1.LSAintro.pdf

2.2. Learn dense vector for a document

2.2.1. Latent semantic analysis

A concept is a relationship among few tokens. The *latent semantic analysis* is a mathematical way to learn these hidden concepts in documents. It is achieved by computing a low-rank representation of a document-token matrix [4, 5, 6]. The singular value decomposition (SVD) is used to achieve it. This decomposition follows the equation:

$$X_{n \times m} = U_{n \times n} \cdot S_{n \times m} \cdot V_{m \times m}^T \tag{5}$$

where n is the number of documents and m is the number of tokens. S is a diagonal matrix containing the singular values in descending order. The singular values are real numbers. It contains the weights of concepts present in the document-token matrix. It has the same shape as the original matrix X. The matrices U and V are the orthogonal matrices and satisfy:

$$U^T \cdot U = I_{n \times n} \tag{6}$$

$$V^T \cdot V = I_{m \times m} \tag{7}$$

where I is an identity matrix. Mathematically, singular values[11] from matrix S are the square roots of the eigenvalues of $X^T \cdot X$ or $X \cdot X^T$. The eigenvectors of $X \cdot X^T$ are the columns of matrix U and the eigenvectors of $X^T \cdot X$ are the columns of matrix V.
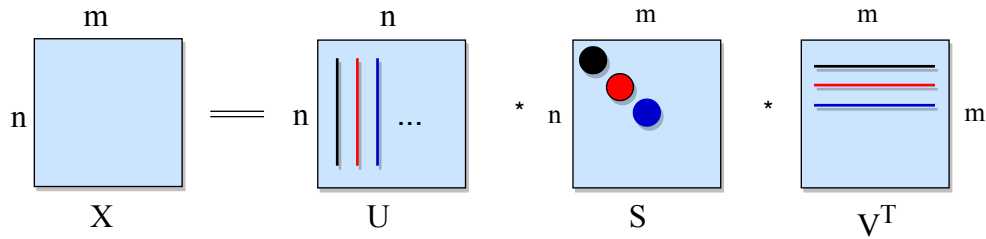
Figure 7.: Singular value decomposition: The image shows how a matrix is decomposed using the singular value decomposition. The matrix X is factorised into three matrices - U, S and V using equation 5. These factor matrices (U, S and V) are used for the low-rank estimation of matrix X.

Figure 7[12] explains how the SVD of a matrix is computed. The matrix U contains information about how the tokens, arranged along the columns, are mapped to concepts. The matrix V stores information about how concepts are mapped to documents which are arranged along the rows.

Low-rank approximation

The document-token matrices suffer from the sparsity and show no relation among tokens. The low-rank approximation of a matrix is important to discard the features which do not repeat. It deals with these issues. The features with smaller singular values (the last entries of the matrix S along the diagonal in equation 5) represent noise and are discarded and the features with larger singular values (the top entries of the matrix S along the diagonal in equation 5) are retained. The resulting low-rank matrices are dense and contain only larger singular values [7]. A low-rank approximation X_k ($k < m$) is computed using equation 8. The size of the reconstructed matrix X remains the same but its rank reduces to k.

$$X_{n \times m} = U_k \cdot S_k \cdot V_k^T \tag{8}$$

where U_k is the first k columns of U, V_k is the first k rows of V and S_k is the first k singular values in S. X_k is called as the rank-k approximation of full-rank matrix X. Figure 9 shows how the fraction of the sum of singular values changes with the fraction of the ranks of document-token matrices. The percentage rank is $k \div K$ where $1 <= k <= K$ and K is the original (full) rank of a matrix. From figure 9, if the ranks of matrices are reduced to 70% of corresponding full-ranks, it is still possible to capture $\approx 90\%$ of the sum of singular values. The reduction to half of the full-ranks achieves $\approx 80\%$ of the sum of singular values. This variation is also shown for input and output file types in figures 8 and 9 but its rank is not reduced. Its plot is added only for completeness.

The ranks of the document-token matrices for name and description and help text attributes are reduced 5% of the corresponding full-ranks. It gives dense, low-rank approximations of these document-token matrices. In these low-rank matrices, the dense vector representations for the documents are shown along the rows and the tokens are arranged along the columns. The similarity (correlation or distance) is computed using similarity measures for each pair of document vectors. There

---

[12]http://theory.stanford.edu/~tim/s15/l/l9.pdf
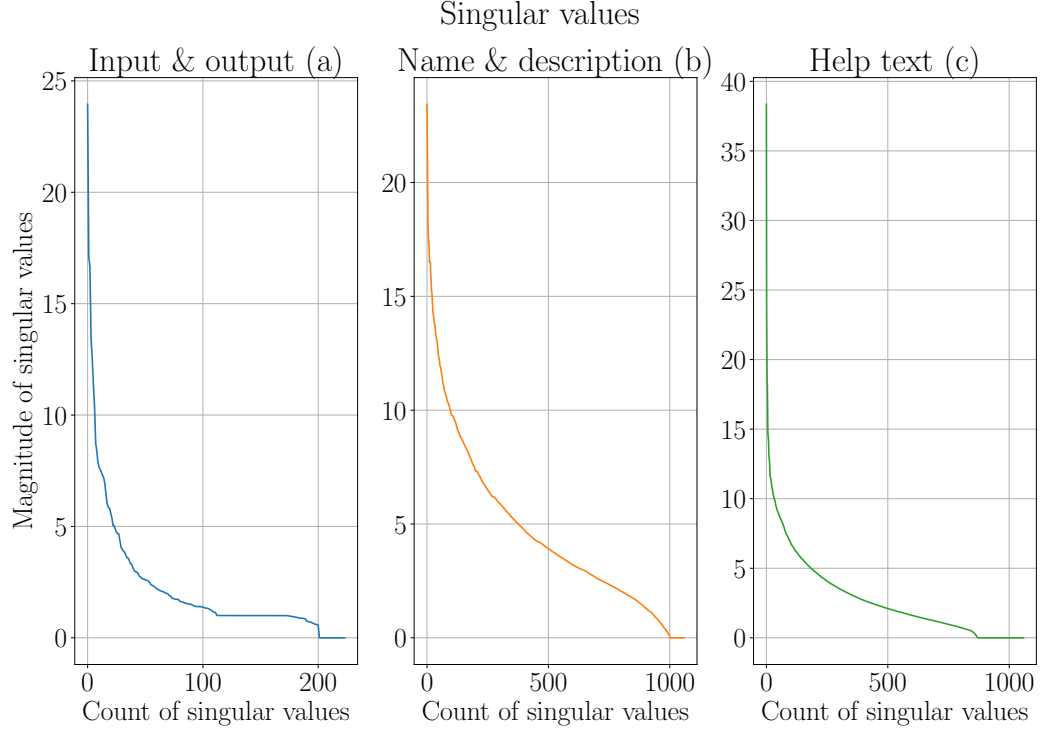
Figure 8.: Singular values of document-token matrices: The plot shows singular values computed using singular value decomposition (equation 5) for document-token matrices of the three attributes (input and output file types (a), name and description (b) and help text (c)). The diagonal matrix S contains the singular values sorted in descending order. The x-axis shows the count of singular values and the y-axis shows the corresponding magnitude. The singular values are always real numbers. In (a), (b) and (c), very few singular values have large magnitude and most of them are small.

are many similarity measures which can be used like the *euclidean distance*, *cosine similarity*, *manhattan distance* or *jaccard index*. In this work, *cosine angle similarity* is used for name and description and help text attributes and *jaccard index* for input and output file types to compute the similarity between each pair of document vectors. A real number between zero and one is assigned as the similarity score for a pair of documents. The higher the score, higher is the similarity between a pair of documents. Computing this similarity for all the documents gives a similarity matrix $SM_{n \times n}$ where n is the number of documents. It is a symmetric matrix (also called the correlation matrix). Three such matrices are computed, each corresponding to one attribute (input and output file types, name and description and help text)

(figures 14, 17 and 20).
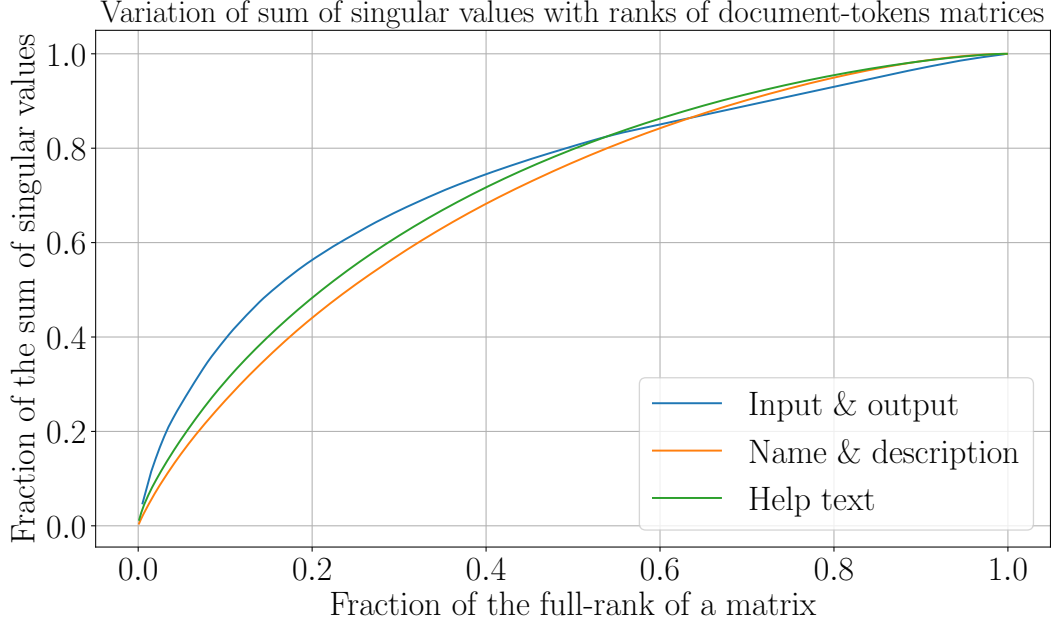
Figure 9.: Variation of the fraction of ranks of document-token matrices with the fraction of sum of singular values: This plot merges the singular values from three different matrices from figure 8 into one plot. As the ranks and sum of singular values of all the document-token matrices vary, they are converted to respective percentages for each matrix. For example, 0.2 on x-axis means 20% of the original rank of a matrix. In equation $rank_{fraction} = \frac{k}{N}$, k is the reduced rank and N is the full-rank of a matrix. Similarly, the y-axis shows the fraction of sum of all the singular values for each matrix. In equation $sum_{fraction} = \frac{\sum_{i=1}^{k} s_i}{\sum_{i=1}^{K} s_i}$, K is the number of all singular values and s_i is the ith singular value. k defines the number of top singular values considered for a document-token matrix when it is reduced to rank k. This plot shows that rank reduction of a document-token matrix is directly proportional to the reduction of the sum of its singular values.

2.2.2. Paragraph vectors

Using the *latent semantic analysis*, dense vectors are learned to represent each document. One limitation of this approach is to assess the quantity by which to lower the ranks of document-token matrices in order to achieve the right document vectors. This factor can be different for different document-token matrices. There are ways to find an optimal rank by optimisation using *frobenius norm* (as a loss

function). But, it is not simple [8]. The weighted similarity scores are dominated by the similarity scores of input and output file types attribute. The similarity scores from the other attributes remain under-represented (section 4.1). Due to these drawbacks, the tools which have similar functions do not get pushed up on the ranking ladder (more similar tools should be at the top of the ranking ladder). To avoid these limitations, an approach known as *doc2vec* (document to vector) [9] is explored. It learns dense, fixed-size vectors for the documents using a neural network. They are unique because they capture semantics present in documents. The documents which share similar context are represented by similar vectors. When cosine distance is computed between these vectors sharing similar context, a higher similarity score is observed. Moreover, it allows documents to have variable lengths.

Approach

It learns vector representations for documents and their words. The words which are used in a similar context have similar vectors. For example, the tokens like *data* and *dataset* are generally used in similar context. Therefore, they are represented by the vectors which are similar. The vector representations of words in a document are learnt by maximising the following function:

$$\frac{1}{T} \cdot \sum_{t=k}^{T-k} \log p(w_t | w_{t-k}, ..., w_{t+k}) \tag{9}$$

where T is the total number of words (w_i) in a document and k is window size. The window size defines a context. A few words, which make a context, are taken and using them, each word is predicted [9]. The probability p is computed using a softmax classifier[13] and backpropagation[14] is used to compute gradient. The stochastic gradient descent is used as an optimiser. The paragraph vectors are used to learn the probability of next words in a context. The dense vectors are learned for each word as well and are known as word vectors. The paragraph and word vectors are averaged or concatenated to make a classifier which predicts next words in a context. There are two ways to choose a context:

- Distributed memory: In this approach, a fixed length window of words are chosen and the paragraph and word vectors are used to predict words in this

---

[13]http://cs231n.github.io/linear-classify/#softmax
[14]http://colah.github.io/posts/2015-08-Backprop/

context. The words vectors are shared across all the paragraphs (documents) and paragraph vector is unique to each paragraph. Figure 10 explains this approach.

Sequence   Classifier

Average/concatenate

Word matrices   W   W   W   D   Paragraph matrix

ART   Illumina   Simulate
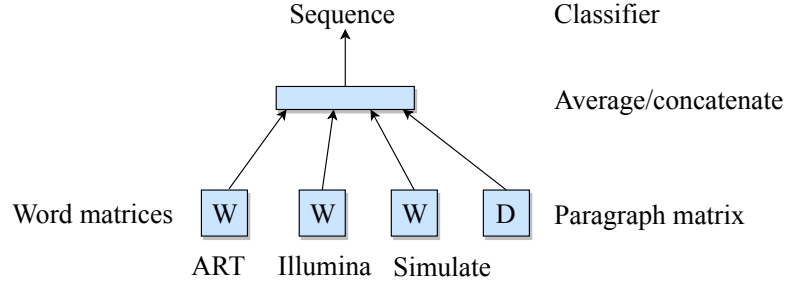
Figure 10.: Distributed memory: The image shows a mechanism for learning paragraph (document) and word vectors. W is a word matrix where each word is represented by a vector. D is a paragraph matrix where each paragraph (document) is represented by a vector. The word vectors are shared across all paragraphs (documents) but not the paragraph vectors. The three words *art, illumina* and *simulate* represent a context. The averaged or concatenated words and paragraph vectors make a classifier which is used to predict the *sequence* word.

- Distributed bag-of-words: In this approach, words are randomly chosen from a paragraph. A word is chosen randomly from the set of words and predicted using paragraph vectors. No order is followed in choosing the words. Figure 11 explains this approach.

ART   Illumina   Simulate   Sequence   Classifier
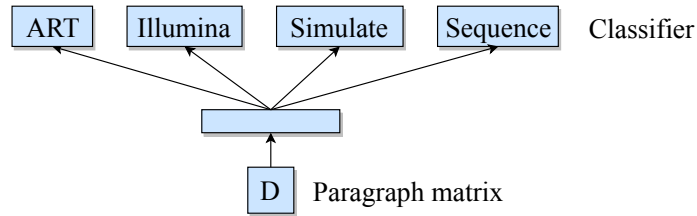
D   Paragraph matrix

Figure 11.: Distributed bag-of-words: The image shows how paragraph vectors are learned by predicting a random word chosen from a randomly selected set of words. D is a paragraph matrix where each paragraph (document) is represented by a vector. In this approach, the order of the words does not matter.

The figures 10 and 11 are inspired by the original work, distributed representations of sentences and document[15]. The second approach of learning paragraph vectors

---
[15]https://arxiv.org/abs/1405.4053

(distributed bag-of-words) is simple and is used to learn document (paragraph) vectors for name and description and help text attributes. Only the paragraph vectors are learned in this approach and the number of parameters is also less than the distributed memory approach. These reasons make it computationally less expensive [9]. The number of parameters is $\approx N \times z$ where N is the number of paragraphs (documents) and z is the dimensionality of each vector.

2.3. Similarity measures

Using the *latent semantic analysis* and *paragraph vectors* approaches, vectors for documents are learned. To find similarity between a pair of vectors, a similarity measure is applied to get a similarity score. This score quantifies how much similar a pair of documents are. In this work, two similarity measures, *cosine similarity* and *jaccard index*, are used. They return a real number between zero and one as a similarity score.

2.3.1. Cosine similarity

It calculates the value of cosine angle between a pair of document vectors. Two vectors, x and y, are taken:

$$x \cdot y = |x| \times |y| \times \cos\theta \tag{10}$$

$$\cos\theta = \frac{x \cdot y}{|x| \times |y|} \tag{11}$$

where $|x|$ is the norm of the vector x. If the norm is zero, $\cos\theta$ is set to zero. $x \cdot y$ is the dot product of the vectors x and y. If the documents are dissimilar, then it is zero and if they are completely similar, it is one. For all the other cases, it stays between zero and one. This score is understood as the probability of similarity between a pair of documents[16].

---

[16]https://nlp.stanford.edu/IR-book/html/htmledition/dot-products-1.html

2.3.2. Jaccard index

Jaccard index is a measure of similarity between two sets of entities and is given by the equation:

$$j = \frac{A \cap B}{A \cup B} \tag{12}$$

where A and B are two sets. $\cap$ is the number of entities present in both sets and $\cup$ is the count of unique entities present in both sets. [10]. This measure is used to compute similarity between two documents based on their file types. For example, a tool *linear regression* has *tabular* and *pdf* as its file types. Another tool *LDA analysis* has *tabular* and *txt* as its file types. *Jaccard index (j)* for the pair of tools is:

$$j = \frac{length[(tabular, pdf) \cap (tabular, txt)]}{length[(tabular, pdf) \cup (tabular, txt)]} = \frac{1}{3} = 0.33 \tag{13}$$

2.4. Optimisation

The similarity matrices are computed by applying similarity measures for each pair of document vectors. These matrices have the same dimensions ($N \times N$, N is the number of documents (tools)). To combine these matrices, a simple idea would be to take an average of the corresponding rows from three similarity matrices. By doing this, the combined similarity scores of one document (tool) with all other documents (tools) are achieved. Iterating this process for all documents gives an average similarity matrix. The diagonal entries of this matrix are one and all the other entries are real numbers between zero and one. A better way to compute the combination of similarity matrices is to learn weights on the corresponding rows from the three matrices. These weights are used to compute the weighted average of the similarity matrices (equation 14). The weights are real numbers between zero and one. For the corresponding rows in similarity matrices, they sum up to one. Instead of using fixed weights (of $1/3 = 0.33$ (3 is the number of similarity matrices)), an optimisation technique is employed to find them. A weighted similarity of a document with all other documents is computed as:

$$SM^k = w_{io}^k \cdot SM_{io}^k + w_{nd}^k \cdot SM_{nd}^k + w_{ht}^k \cdot SM_{ht}^k \tag{14}$$

where each weight (w) is a positive, real number and satisfies $w_{io}^k + w_{nd}^k + w_{ht}^k = 1$. SM_{io}^k, SM_{nd}^k and SM_{ht}^k are similarity scores (matrix rows) for input and output

file types, name and description and help text attributes respectively for the kth document. The similarity scores, SM, has a dimensionality of $1 \times N$ where N is the number of documents. The scores in the similarity matrices are independent of one another. The gradient descent optimiser is used to learn the weights by minimising an error function. The ideal similarity values are set based on similarity measures and are used to define an error function. The maximum similarity between a pair of documents can be one as the values from the *cosine distance* and *jaccard index* can be at most one.

$$SM^k_{ideal} = [1.0, 1.0, ..., 1.0]_{1 \times N} \tag{15}$$

where SM_{ideal} is ideal similarity scores of a document against all other documents and N is the number of documents. Using the ideal and computed similarity scores, mean squared error is computed (equations 16-18) for all three attributes. The attribute which measures lower error should get a higher weight and the attribute which measures higher error should get a lower weight.

2.4.1. Gradient descent

Gradient descent is a popular algorithm for optimising an objective function with respect to its parameters. In this work, weights are learned by minimising mean squared error function:

$$Error_{io}(w^k_{io}) = \frac{1}{N-1} \cdot \sum_{j=1, j \neq k}^{N} (w^k_{io} \cdot SM^j_{io} - SM_{ideal})^2 \tag{16}$$

$$Error_{nd}(w^k_{nd}) = \frac{1}{N-1} \cdot \sum_{j=1, j \neq k}^{N} (w^k_{nd} \cdot SM^j_{nd} - SM_{ideal})^2 \tag{17}$$

$$Error_{ht}(w^k_{ht}) = \frac{1}{N-1} \cdot \sum_{j=1, j \neq k}^{N} (w^k_{ht} \cdot SM^j_{ht} - SM_{ideal})^2 \tag{18}$$

$$Error(w^k) = Error_{io}(w^k_{io}) + Error_{nd}(w^k_{nd}) + Error_{ht}(w^k_{ht}) \tag{19}$$

$$\underset{w^k}{\arg\min} \, Error(w^k) \tag{20}$$

20

$$w^k = w_{io}^k + w_{nd}^k + w_{ht}^k = 1 \tag{21}$$

In equations 16-19, the subscripts *io*, *nd* and *ht* refer to input and output file types, name and description and help text respectively. Each weight term in equation 21 is a real number between zero and one. To minimise the equation 20 under the constraint given by equation 21, the gradient (partial derivative) of the error function is calculated (equation 22). The gradient specifies the rate of change of error with respect to weights.

$$Gradient(w^k) = \frac{\partial Error}{\partial w^k} = \frac{2}{N-1} \cdot \sum_{t=1, t \neq k}^{N} (w^k \cdot SM^t - SM_{ideal}) \cdot SM^t \tag{22}$$

The *Gradient* is a vector $(Gradient_{io}, Gradient_{nd}, Gradient_{ht})$. Using this gradient vector, weights are updated for each attribute. The weight update equation (23) needs a learning rate η.

$$w^k = w^k - \eta \cdot Gradient(w^k) \tag{23}$$

where η is the learning rate.

2.4.2. Learning rate decay

Finding a good learning rate is an important part of gradient descent optimisation. If it is high, it poses a risk of optimiser divergence. On the other hand, if it is small, the optimiser can take a long time to converge. Both these situations are undesirable and should be avoided by starting off with a small learning rate and gradually decrease it over iterations. The decay is important because as learning saturates, only small steps towards the minimum (of error function) are needed to converge. This technique is called time-based decay [11]. Figure 12 shows the decay of learning rate over iterations. Equation 24 is used to decay the learning rates shown in figure 12.

$$lr^{t+1} = \frac{lr^t}{(1 + (decay * iteration))} \tag{24}$$

where lr^{t+1} and lr^t are learning rates for $t+1$ and t iterations respectively, *decay* controls how steep or flat the learning rate curve is and *iteration* is an iteration

number. A high value of decay can make the learning rate drop quickly. A low value can make the curve flat which can slow down the learning.
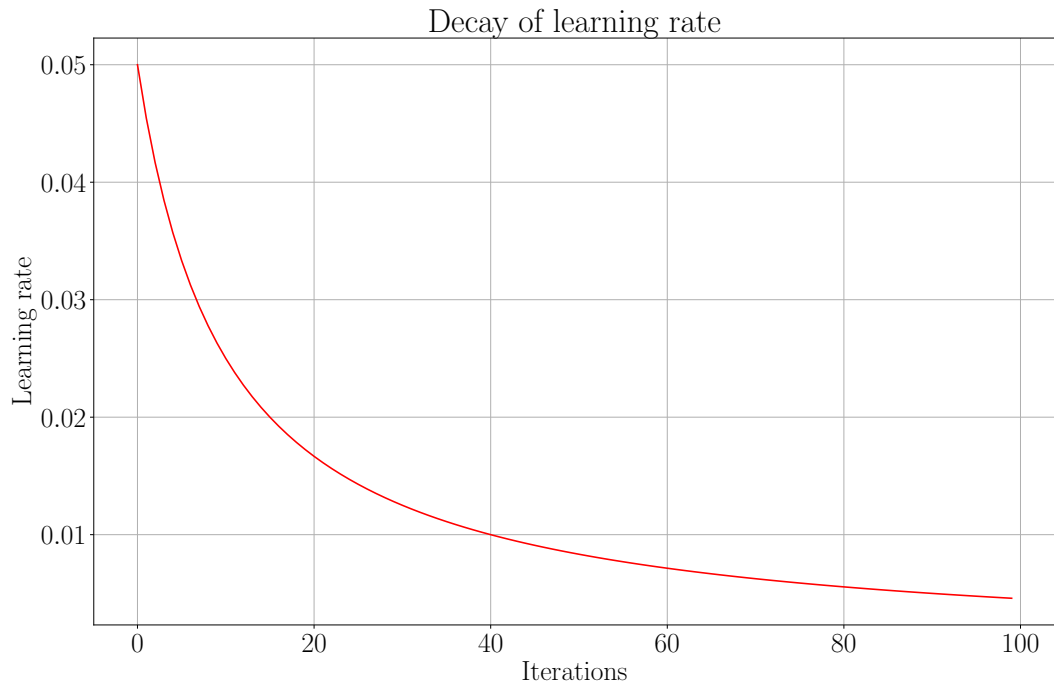
Figure 12.: Decay of learning rate for gradient descent optimiser: The plot shows how the learning rate for gradient descent changes with the iterations. It starts with a small value and decreases gradually over time. It is essential to have the learning rates which neither drops too quickly nor drops too slowly. Both of these ways can lead to the divergence or slow convergence of the optimiser.

2.4.3. Weight update

Momentum

To reach the minimum point of an error function (equation 20), an optimiser should go down continuously without being blocked at saddle points. At these points, the derivative of a function is zero. Adding a momentum term to weights avoids these saddle points and an optimiser converges to the lowest point quickly. It gives a necessary push to keep going down the error function by adding a fraction of the previous update to the current update [11, 12]. The weight is updated for each iteration using:

$$update_{t+1} = \gamma \cdot update_t - \eta \cdot Gradient(w_t) \qquad (25)$$

$$w_{t+1} = w_t + update_{t+1} \qquad (26)$$

where $update_{t+1}$ is the update for changing weights for current iteration $t + 1$. $update_t$ is the previous update. η is learning rate and $Gradient$ is with respect to weight w_t. γ specifies the fraction of previous update to be used.

Nesterov's accelerated gradient

The inclusion of momentum is useful to get necessary advance towards finding the minimum of the error function. However, the speed of going down the slope of an error function should become less if there is a possibility of change in gradient direction. In this situation, the speeding up can be avoided by estimating the forthcoming gradient (gradient for next step) and then correcting it [13]. The weight is updated for each iteration using:

$$update_{t+1} = \gamma \cdot update_t - \eta \cdot Gradient(w_t + \gamma \cdot update_t) \qquad (27)$$

$$w_{t+1} = w_t + update_{t+1} \qquad (28)$$

The meaning of the terms remains same as in the previous equations 25 and 26.

Gradient verification

To verify that the gradient computed using partial derivative is correct, an approximated gradient (linear approximation) is computed using equation 29. The difference between these two variants should be close to zero.

$$Gradient(w) = \frac{\partial Error}{\partial w} \approx \frac{Error(w + \epsilon) - Error(w - \epsilon)}{2 \cdot \epsilon} \qquad (29)$$

where ϵ is a very small number ($\approx 10^{-4}$). Figure 13 shows the difference of the actual (using partial derivative) and approximated (linear approximation using error function) gradients for all three attributes.
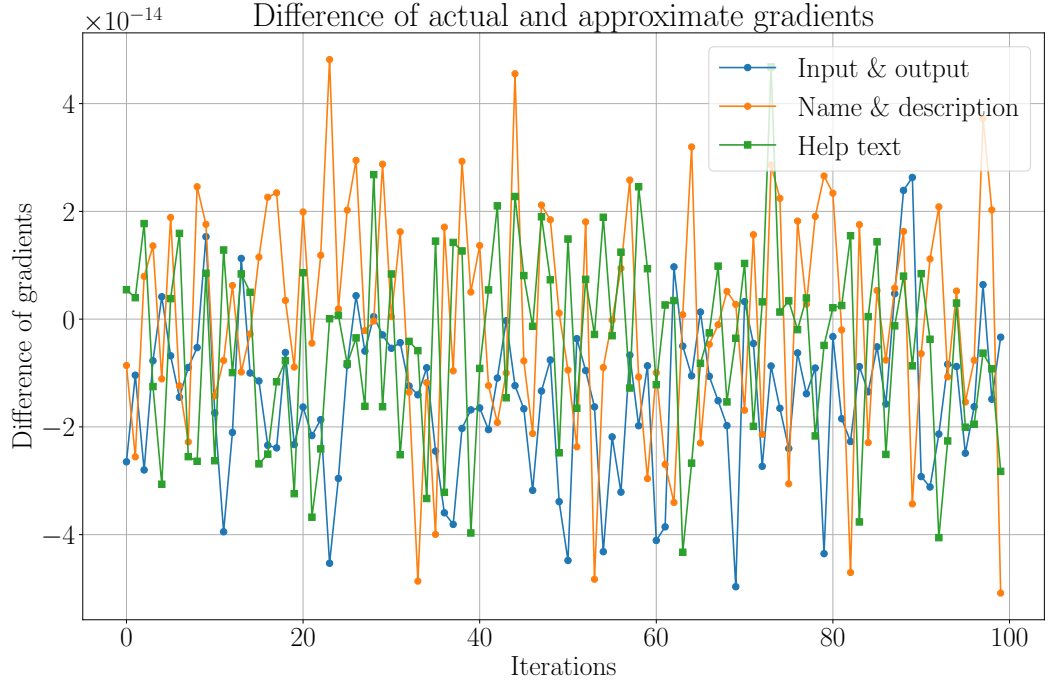
Figure 13.: Difference between actual and approximated gradients: The plot shows a difference between actual and approximated gradients. They are computed for three attributes and averaged for all tools over 100 iterations of optimisation. The difference of the gradients is consistent $\approx 10^{-14}$ which means that the actual and approximated gradients are same. It proves that gradients computed using partial derivatives are correct.

3. Experiments

3.1. Number of attributes

Three different attributes, input and output file types, name and description and help text, are used for compiling metadata of tools. The idea to use them together to make one set of tokens for each tool is not beneficial. Instead, similarities are computed using these attributes separately and are combined using optimisation.

3.2. Amount of help text

The help text attribute is noisy and contains text (partly) which is not useful for finding similarity among tools. Therefore, only the first four lines of text are used from this attribute.

3.3. Similarity measures

Jaccard index is used as a similarity measure for input and output file types attribute and cosine angle similarity is used for name and description and help text attributes. They give a real number between zero and one as a similarity score for each pair of tools.

3.4. Latent semantic analysis

Using *latent semantic analysis*, dense vectors are learned for each document by reducing the ranks of document-token matrices. They are reduced to 5% of the full-ranks of document-token matrices. The document-token and similarity matrices are expected to be denser compared to no rank reduction. Only the document-token matrices of name and description and help text attributes are considered for low-rank

estimation. The singular value decomposition method is used from its implementation in *numpy*[1] linear algebra package.

3.5. Paragraph vectors

The fixed-length, dense vectors (also called paragraph vectors) are computed for name and description and help text attributes. When the number of tokens for a tool is lower, a lower number of dimensions is used for dense vectors. Figure 5 shows that the number of tokens is higher for help text than name and description. Therefore, the dimension is set to 100 and 200 for name and description and help text respectively. The window size for sampling text is 5 for name and description and 15 for help text. The neural network is iterated over 10 epochs and each epoch has 800 iterations. In each epoch, all tools are used for training. A python implementation of this approach, *gensim*[2], is used to learn these vectors. Out of the two approaches (*distributed memory* and *distributed bag-of-words*) to learn paragraph vectors, *distributed bag-of-words* approach is applied to learn these vectors. It does not compute word vectors which makes it computationally less expensive.

3.6. Gradient descent

It is used to optimise the combination of similarity scores computed from three attributes by learning weights on the similarity scores. Based on similarity measures, an error function is defined for the optimiser. It executes for 100 iterations to stabilise the error drop. The *nesterov's accelerated gradient* is used to ensure a steady drop in error. A time-based decay strategy is implemented to decay the learning rate after each iteration of gradient descent. The drop in the learning rate is kept steady. The initial value is set to 0.05.

---

[1]https://docs.scipy.org/doc/numpy-1.14.0/reference/generated/numpy.linalg.svd.html

[2]https://radimrehurek.com/gensim/models/doc2vec.html

4. Results and analysis

4.1. Latent semantic analysis

The document-token matrices of the name and description and help text attributes are made denser by reducing their ranks. It allowed the corresponding similarity matrices to become denser too. Due to this, larger weights are learned on the similarity matrices by an optimiser. The rank reduction is not applied to the document-token matrix of the input and output file types. It is not beneficial to find out any correlation among the file types.

4.1.1. Full-rank document-token matrices

Figure 14 shows the similarity matrices computed using the full-rank document-token matrices for the input and output (14a), name and description (14b) and help text (14c) attributes. Using these similarity matrices, weights are learned using gradient descent optimiser. The similarity matrices and weights (figure 15) are combined to get a weighted average similarity matrix (14d). The weights for the input and output file types are larger than that of the other two attributes. It is associated with the larger values in the corresponding similarity matrix. The average of weighted similarity is computed using the weights learned by the optimiser (optimal weights) and uniform weights ($\frac{1}{3}$) where 3 is the number of attributes. It is shown in figure 16. A row-wise average is computed from the weighted similarity matrix (in figure 14d) to get an average of weighted similarity with optimal weights. The similarity matrices from 14a, 14b and 14c are combined using uniform weights and then, a row-wise average is computed to get average of weighted similarity using uniform weights.

Similarity matrices
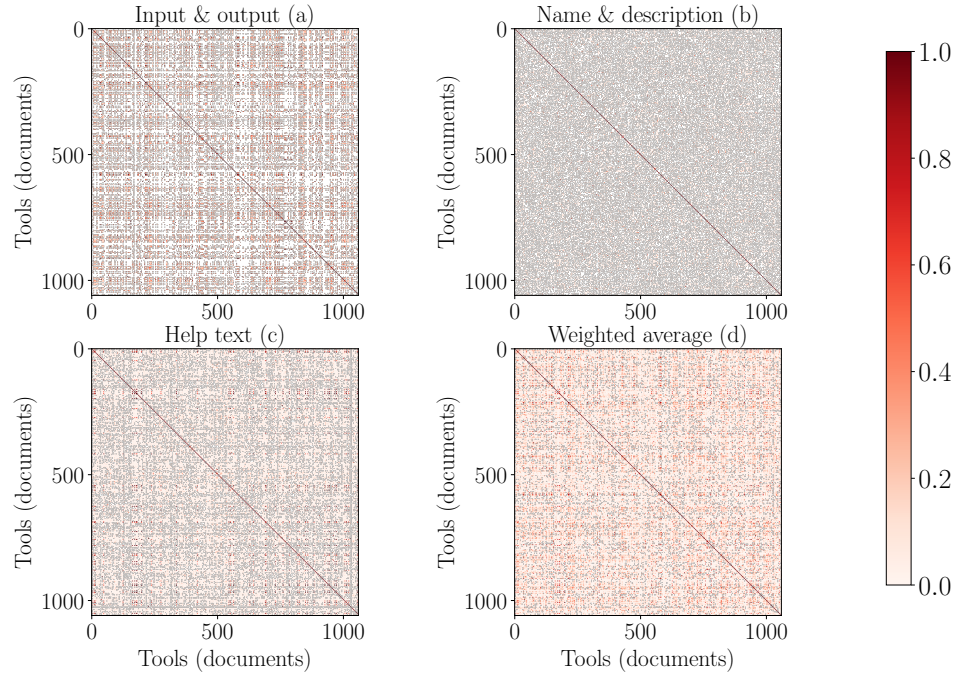
Figure 14.: Similarity matrices computed using full-rank document-token matrices: The heatmaps show the similarity matrices for the input and output file types (a), name and description (b) and help text (c) attributes. The subplot (d) shows a weighted average of the similarity matrices computed in (a), (b) and (c). The weights used in computing (d) are shown in figure 15. The document-token matrices corresponding to the similarity matrices have their full-ranks.
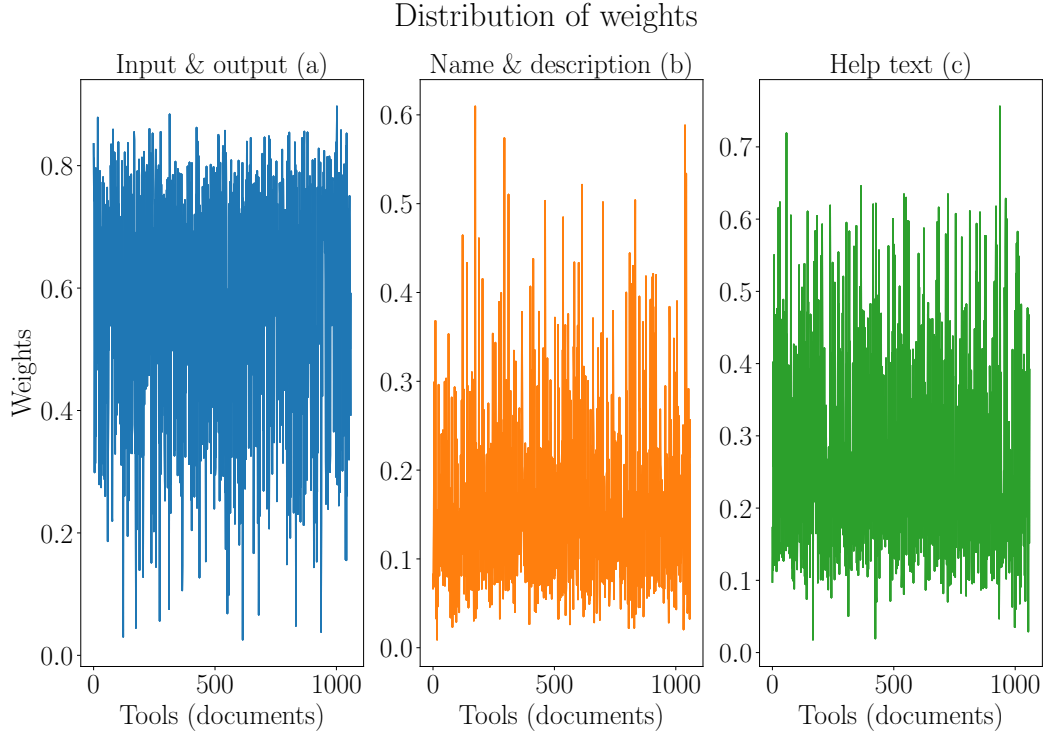
Figure 15.: Distribution of weights learned for similarity matrices computed using full-rank document-token matrices: The plot shows the distribution of weights learned for the similarity matrices in 14a, 14b and 14c by the gradient descent optimiser for different attributes. The larger weights are learned for the input and output file types attribute (a) compared to the name and description (b) and help text (c) attribute.
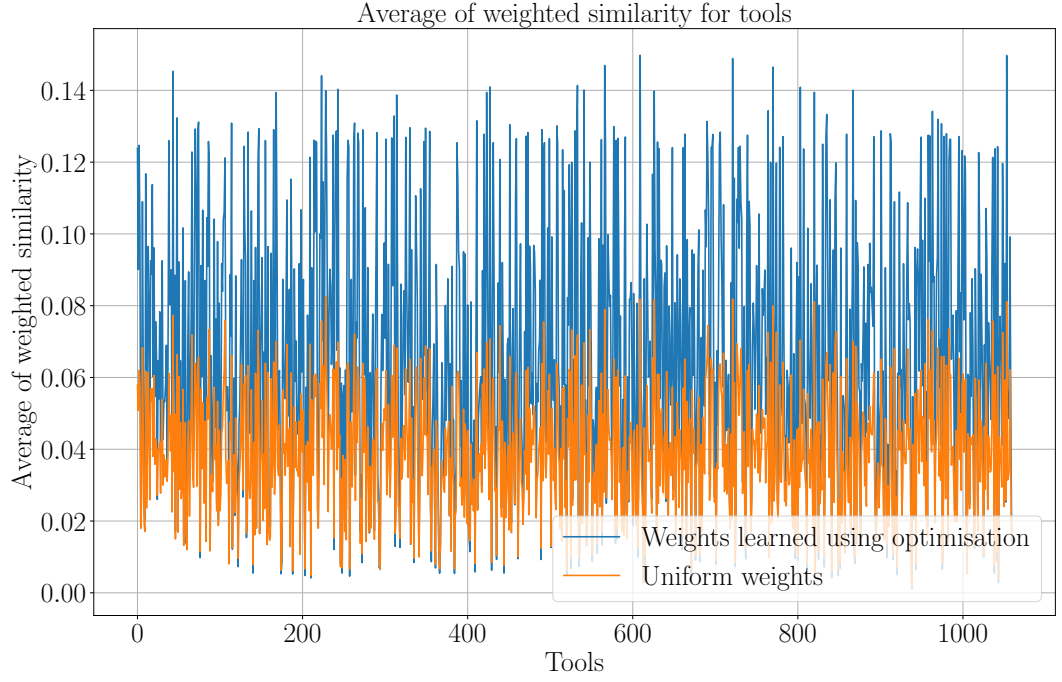
Figure 16.: Average similarity computed using uniform and optimal weights: The plot shows the average weighted similarity computed using the uniform and optimal weights (learned by the optimiser). The full-rank document-token matrices are used. The average similarity computed using optimal weights is larger than uniform weights.

4.1.2. 5% of full-rank

The ranks of the document-token matrices for the name and description and help text attributes are reduced to 5% of their corresponding full-ranks. By choosing this low value, only the top $\approx 20\%$ of the sum of singular values is considered (figure 9). Figure 17 shows that the corresponding similarity matrices become denser compared to figure 14. The larger weights are learned for the name and description (18b) and help text (18c) than that of the input and output file types (18a) attribute. An average of the weighted similarity is computed (figure 19). The same approach is used to compute it as explained in section 4.1.1.
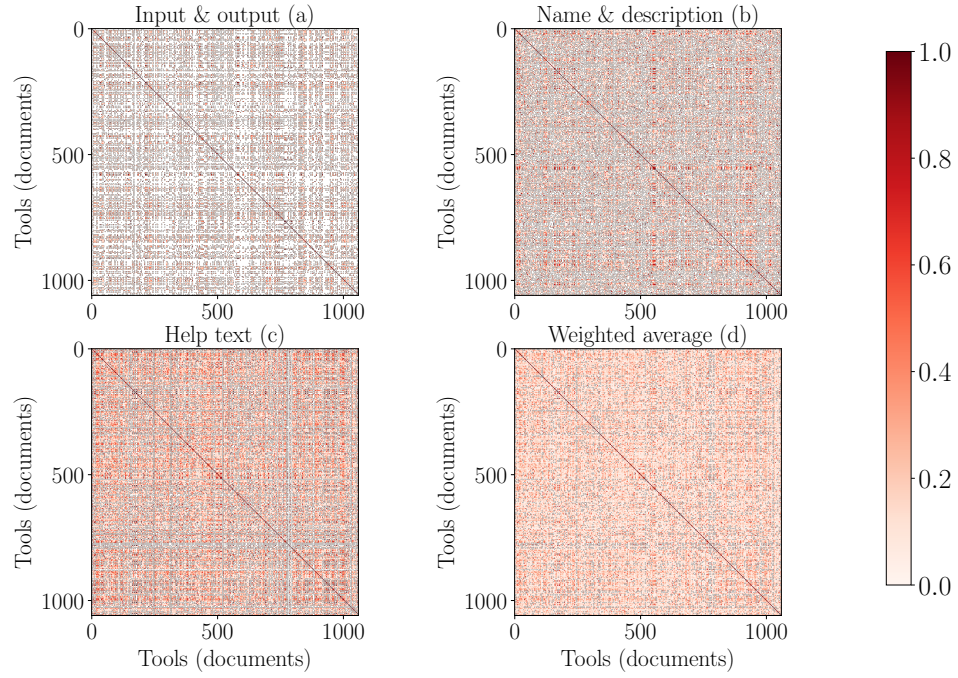
Figure 17.: Similarity matrices computed using document-tokens matrices reduced to 5% **of their full-rank**: The heatmaps show the similarity matrices for the input and output file types (a), name and description (b) and help text (c) attributes. The subplot (d) shows the weighted average of the similarity matrices computed in (a), (b) and (c). The document-token matrices are reduced to 5% of their corresponding full-ranks. The similarity matrices in (b) and (c) are denser than those in 14b and 14c respectively. The weights used in computing (d) are shown in figure 18.
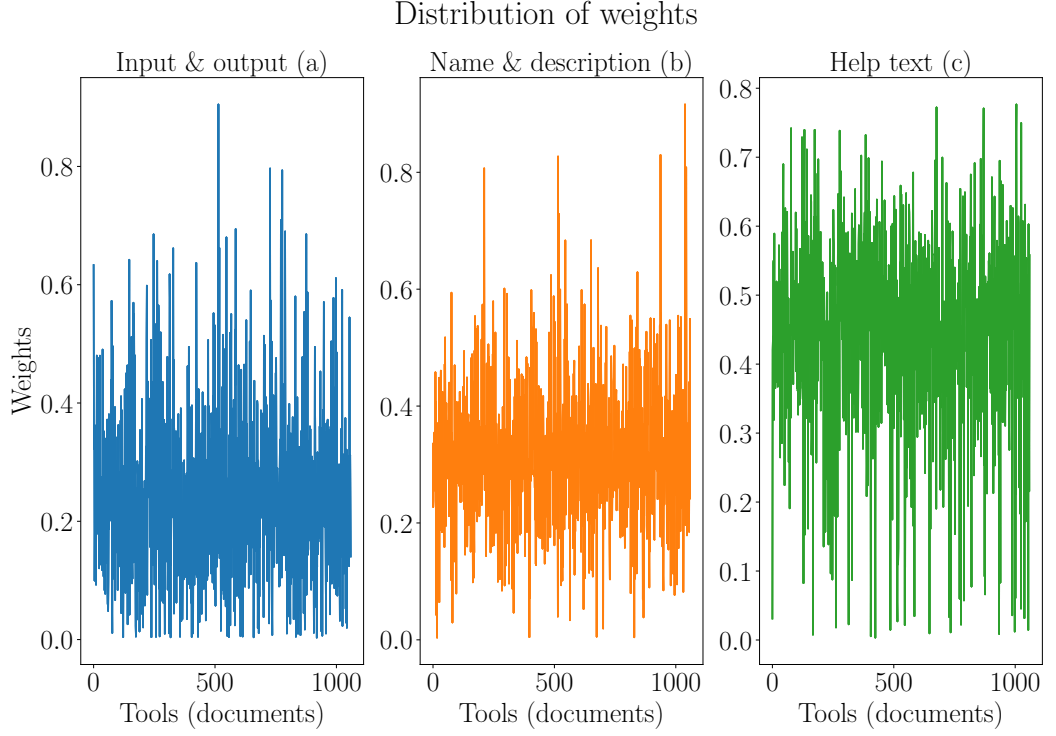
Distribution of weights

Input & output (a)   Name & description (b)   Help text (c)

Figure 18.: Distribution of weights learned for similarity matrices computed using document-token matrices reduced to 5% **of their full-rank**: The plot shows the distribution of weights learned for the similarity matrices (17a, 17b and 17c) by the gradient descent optimiser. The corresponding document-token matrices contain 5% of their full-ranks. The larger weights are learned for the name and description (b) and help text (c) attributes compared to figure 15b and 15c. The weights decrease for the input and output file types (a) attribute compared to 15a.
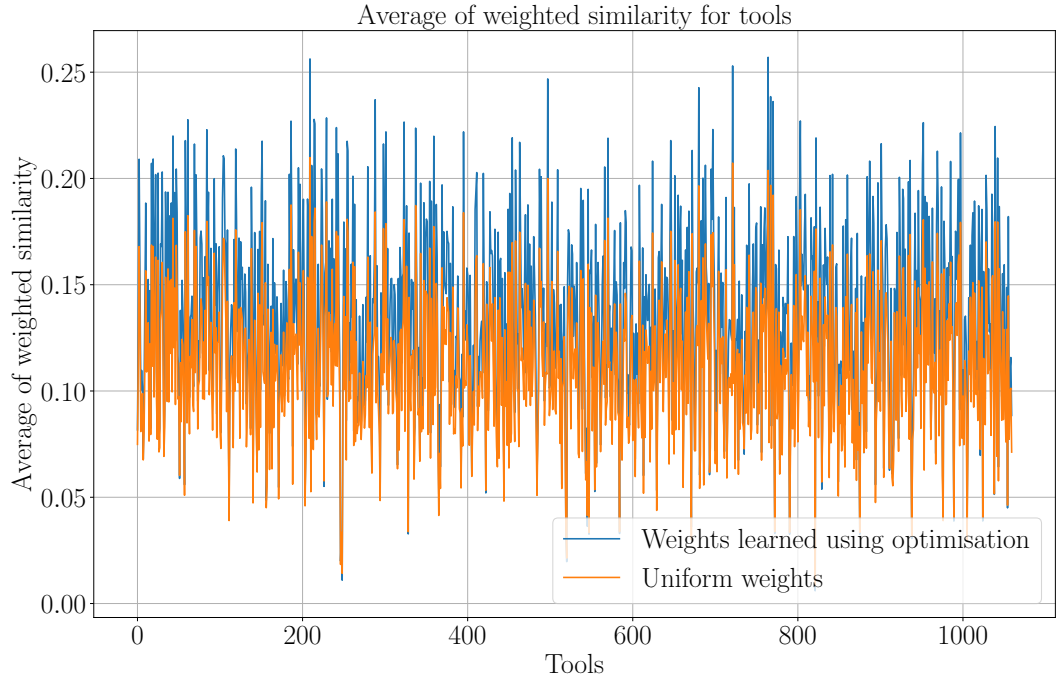
Figure 19.: Average similarity computed using uniform and optimal weights: The plot shows the average weighted similarity computed using the uniform and optimal weights. The document-token matrices are reduced to 5% of the full-rank. The average similarity scores computed using optimal weights are larger than using uniform weights. Compared to figure 16, it measures larger similarity scores.

4.2. Paragraph vectors

The paragraph vectors approach is used to learn a fixed-length, multi-dimensional vector for each document from the name and description and help text attributes. Using their document-token matrices, the similarity matrices are computed (figure 20). These similarity matrices are symmetric and dense. Larger weights are learned for the name and description (21b) and help text (21c) compared to the input and output file types (21a). Figure 22 shows that the average weighted similarity scores across all the tools are also larger compared to that of the *latent semantic analysis* approaches (figures 16 and 19). The average weighted similarity increases to ≈ 0.30 using optimal weights. For the uniform weights as well, the average similarity is ≈ 0.25 (figure 22).
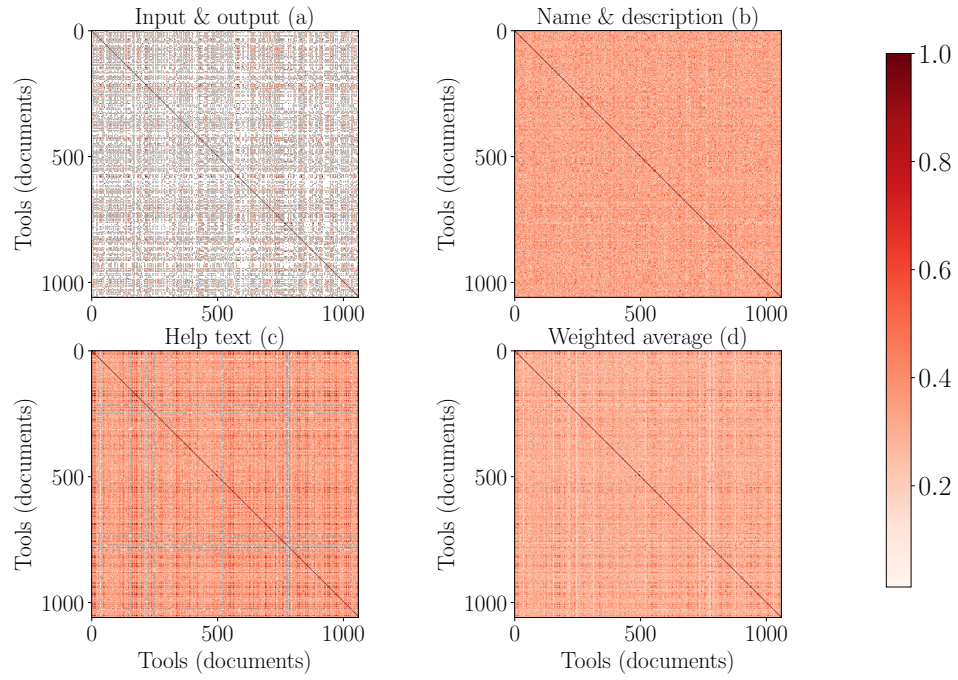
Figure 20.: Similarity matrices using paragraph vectors approach: The heatmaps show the similarity matrices for the input and output (a), name and description (b) and help text (c) attributes. The subplot (d) shows a similarity matrix which is the weighted average computed using (a), (b) and (c). The weights used in computing the weighted average similarity matrix in (d) are shown in figure 21. The similarity matrices (b), (c) and (d) are denser than those in figures 14 and 17.

Distribution of weights
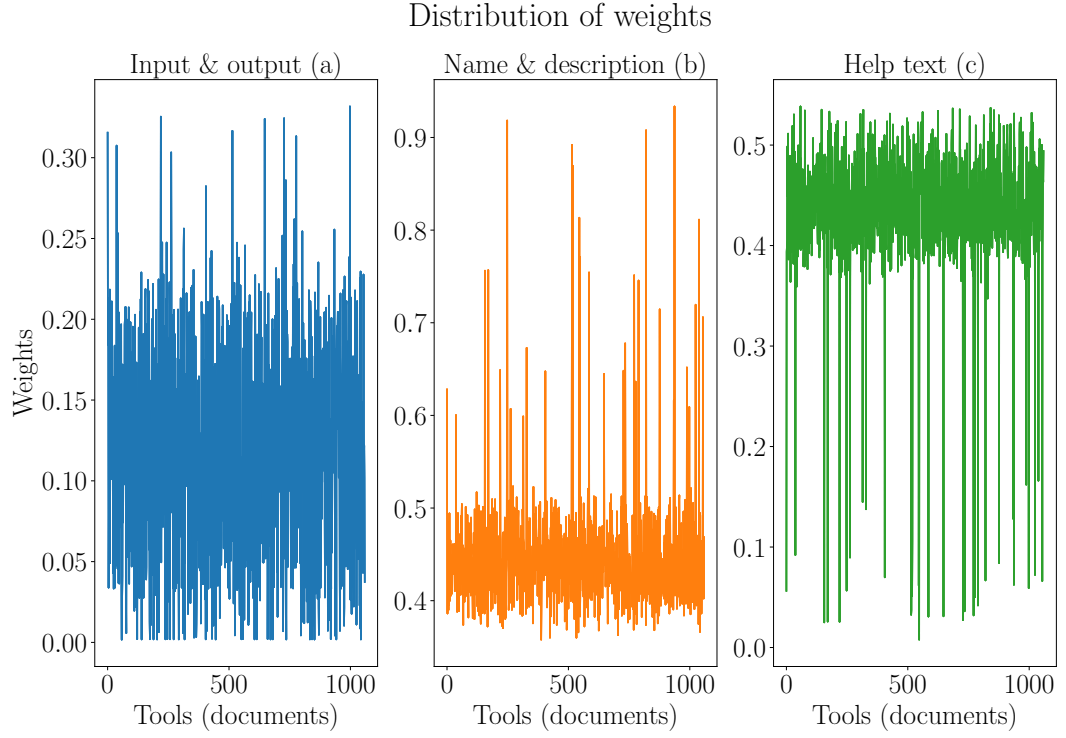
Figure 21.: Distribution of weights for similarity matrices computed using paragraph vectors approach: The plot shows the distribution of weights learned by the gradient descent optimiser on the similarity matrices (20a, 20b and 20c) for the input and output file types (a), name and description (b) and help text (c) attributes. The weights for the name and description and help text attributes are larger than that of the input and output file types attribute.
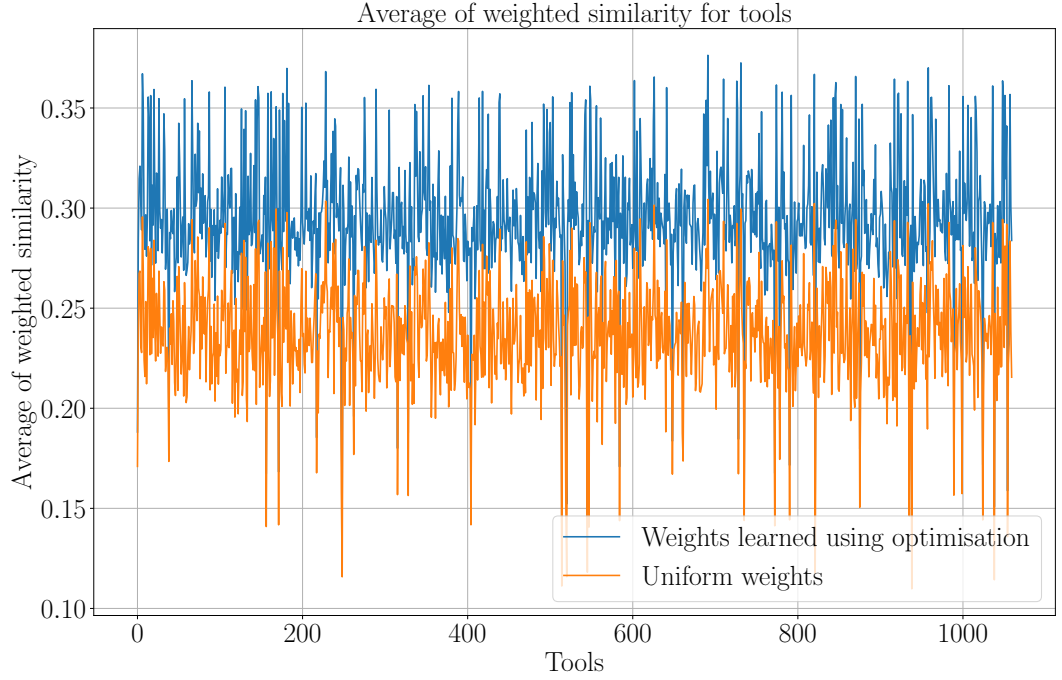
Figure 22.: Average similarity computed using uniform and optimal weights: The plot shows a comparison of the average weighted similarity scores computed using the optimal and uniform weights across all the tools. The average similarity scores using the optimal weights are larger than using the uniform weights. It learns larger similarity scores using uniform and optimal weights than the *latent semantic analysis* approach (figures 16 and 19).

4.3. Comparison of latent semantic analysis and paragraph vectors approaches

A comparison is done between the similar tools assessed by the two approaches used in this work. The similar tools for *hisat* are computed. Two similar tools for *hisat* are computed, once with the full-rank document-token matrices (table 2) and again with 5% of the full-rank document-token matrices (table 3). Moreover, to compare with the *paragraph vectors* approach, two similar tools for *hisat* are computed (table 4). Using the tables 2, 3 and 4, the similar tools for *hisat* are analysed with their respective similarity scores for the different attributes. The description below each table gives the values of the optimal weights (learned by the optimiser). For example,

the weighted similarity score in the first row of table 2 is calculated using the following equation (equation 30).

$$0.38 \cdot 0.77 + 0.10 \cdot 0.07 + 0.13 \cdot 1.0 = 0.42 \tag{30}$$

From the tables 2, 3 and 4, it is concluded that the *paragraph vectors* approach works better than the *latent semantic approach*. In table 2, for the name and description column, the similarity values are too less (0.07 and 0.12 for *hisat2* and *srma_wrapper* respectively). In table 3, the similarity scores for the name and description are not correct as they measure 1.0 even though their descriptions are not exactly same. These incorrect interpretations can lead to wrong similarity assessment. As the low-rank estimation of the input and output file types document-token matrix is not done, its score remains the same in table 2 and 3. The *hisat2* has the same score for the input and output column in all the tables (2, 3 and 4). However, in table 4, the similarity scores seem to be reasonable, neither too high and nor too low. The similar tool ranked second (*tophat*) in table 4 is more relevant than those from the tables 2 and 3.

Similar tools	Input & output	Name & desc.	Help text	Weighted similarity
hisat2	0.38	0.07	1	0.42
srma_wrapper	0.5	0.12	0.01	0.4

Table 2.: Similar tools (top-2) for *hisat* computed using full-rank document-token matrices: The table shows top-2 similar tools selected for *hisat*. This set of similar tools uses full-rank document-token matrices. The weights learned by optimisation are 0.77 (input and output file types), 0.10 (name and description) and 0.13 (help text).

Similar tools	Input & output	Name & desc.	Help text	Weighted similarity
hisat2	0.38	1	1	0.83
srma_wrapper	0.5	1	0.64	0.69

Table 3.: Similar tools (top-2) for *hisat* computed using document-token matrices reduced to 5% of full-rank: The table shows top-2 similar tools selected for *hisat*. This set of similar tools uses document-token matrices reduced to 5% of full-rank. The weights learned by optimisation are 0.27 (input and output file types), 0.23 (name and description) and 0.5 (help text).

Similar tools	Input & output	Name & desc.	Help text	Weighted similarity
hisat2	0.38	0.46	1	0.67
tophat	0.25	0.73	0.54	0.58

Table 4.: Similar tools (top-2) for *hisat* computed using paragraph vectors approach: The table shows top-2 similar tools selected for *hisat*. The weights learned by optimisation are 0.14 (input and output file types), 0.44 (name and description) and 0.42 (help text).

5. Conclusion

5.1. Tools data

The help text attribute was noisy containing a lot of words which were generic and provided little information to identify the tools. On the other hand, it was necessary for the analysis as it supplied more metadata. Therefore, it needed more filtering than the other attributes. Only the first four lines of text were taken for the analysis from the help text. The metadata from the input and output file types and name and description was helpful. The extraction of metadata from the *github's* multiple repositories was slow[1]. Therefore, the metadata from the XML files was read into a tabular file and it was used as the data source for this analysis.

5.2. Approaches

Two approaches were investigated to find similar tools. The *latent semantic analysis* approach relied on matrix rank reduction of the documents-token matrices. It removed unimportant dimensions and worked better than using the full-rank documents-token matrices. However, due to the lack of knowledge of the exact amount of rank reduction, the loss of important dimensions was risked. During optimisation, more importance was given to the input and output file types which were many times undesirable. But, this approach was simple and took less time (≈ 350 seconds for $\approx 1,050$ tools) to complete. The low-rank estimations of the sparse document-token matrices were easily computed using singular value decomposition.

The *paragraph vectors* approach worked in a more robust way than the *latent semantic analysis* approach to find similar tools. The vectors it learned for the name and description and help text were dense. The documents which were similar in context learned similar vectors. However, this approach was slow as it took $\approx 1,000$ seconds to finish. Most of the time was spent to learn the document vectors. It

---

[1]The extraction of $\approx 1,050$ tools took ≈ 30 minutes

achieved higher average weighted similarity scores than the *latent semantic analysis* approach (figure 19 and 22).

5.3. Optimisation

Learning weights on similarity scores worked in a stable way and reached the saturation point already before the 50th iteration. Therefore, the number of iterations for the gradient descent can be reduced from 100 to ≈ 50. The gradient descent optimiser was used with mean squared error as the loss function. Mean squared error was used because the hypothesis similarity scores distribution needed to be as close to the true distribution (based on the similarity measures) as possible. The risk of getting stuck at saddle points or local minima was reduced by using momentum with an accelerated gradient to update the weights.

6. Future work

6.1. Get true similarity values

To quantify the improvements in the ranking of the similar tools for a tool, true similarity scores should be set for each pair of tools. For example, a dictionary of 10 similar tools can be created for each tool. Then, the computed similar tools can be verified against this true set of similar tools. Otherwise, it is required to have a visualiser to look through the similar tools. It would ensure whether the approaches actually work in finding similar tools. At the same time, it is not an easy task to create these logical categories and define similarity scores within these categories.

6.2. Exclude low similarity scores

The similarity matrices were dense. The low scores from the similarity matrices can be excluded to retain only the high scores. One way is to find the median of scores for a tool. The similarity scores lower than the median can be set to zero. Then, the optimisation would use only the important scores to compute and minimise the error.

6.3. Different error functions

Mean squared error was used as a loss function for the optimiser. Other error measures like the *cross-entropy* can be used. With a new error function, it is necessary to redefine the true similarity value which would depend on the similarity measures. The different similarity measures like the *euclidean distance* can be used as well.

6.4. More tools

The number of tools to do the analysis on can be increased. It would provide more data and consequently, more context to learn better semantics in the documents.

6.5. Learn tool similarity using workflows

It can be assumed that the tools which are similar are used in similar context in workflows. It means that similar tools are used for similar kind of data processing. This concept can be used to assess similar tools. The distributed memory approach learns vectors for words in a document. The document can be replaced by paths extracted from the workflows and tools can replace the words. Then, dense vectors for tools can be learned. The tools which are used in the similar context would learn similar vectors.

Part II.

Predict next tools in scientific workflows

7. Introduction

7.1. Galaxy workflows

A Galaxy workflow is a sequence of scientific tools to process biological data. The tools are connected one after another forming a data processing pipeline. Adjacent tools are connected through compatible data types which means that the output data type of one tool is consumed by its next tool. A workflow is a directed acyclic graph (figure 23). It can have multiple paths between its input and output tools and these paths can have one or more tools in common. Each path has a direction commencing from an input tool and ending at an output tool. In figure 23, the tools like *get flanks*, *AWK* and *intersect* are common in both the paths.
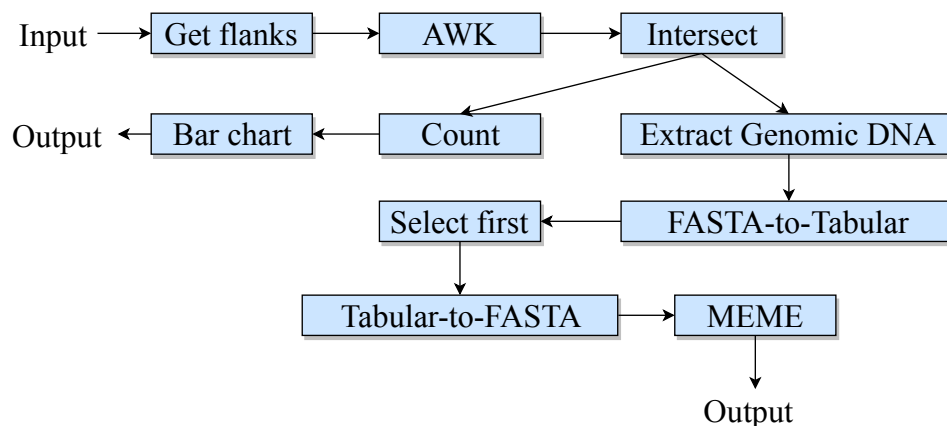
Figure 23.: **A workflow**: The image shows a workflow with two paths. It takes input data, processes it through multiple steps involving many tools and gives two outputs.

To create a workflow, a tool is chosen from the cluster of tools and is connected to the previous one. At each step, a tool can connect to one or more tools which are compatible with the previous one. The decision to select a tool may depend on several factors like the kind of input data or data-processing required to attain the desired output.

7.1.1. Motivation

To create a workflow, having multiple paths where each path can have many tools, is a complex task. A user needs to have knowledge of the tools that should come next. These next tools must be compatible with the previous tool. No two incompatible tools can connect to each other on the canvas of Galaxy workflow editor. This knowledge of compatibility can be gained only through experience. A user who is new to the Galaxy platform and is not aware of the existing tools, creating a workflow can be a laborious and time-consuming effort.

Input ⟶ Get flanks ⟶ AWK ┈ Intersect
                              ┈ Subtract
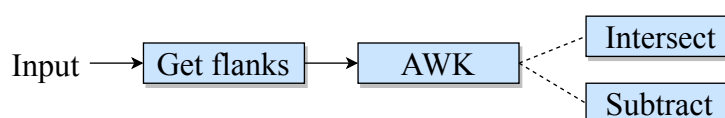
Figure 24.: Multiple next tools: The image shows a part of a workflow where one tool can connect to multiple tools.

In figure 24, a tool *AWK* can connect to two tools, *intersect* and *subtract*. The number of next tools for any tool can vary. Some tools can have just one next tool but others can have multiple next tools. To impart the knowledge of next tools (for a path) and assist a user at each step of creating a workflow, a predictive system to recommend next tools is proposed. It would recommend a set of next possible tools to a user whenever he/she chooses or connects a tool to a tool. It would present the most probable set of next tools making it easier to create a workflow. A reduction in the amount of time taken to create workflows is also expected.

8. Related work

Paths extracted from the workflows are sequential in nature as the tools are connected one after another. In order to predict the next tools, all the previous connected tools should be taken into account. As the workflows possess long sequences of tools, it becomes important to explore some works from the machine learning field which analyse similar data. Interestingly, learning from sequential data is a popular task in many other fields like natural language processing [14, 15], clinical data analysis [16] and speech processing [17, 18].

In the natural language processing field, deep learning models are used to learn sequences of words which aim to categorise a corpus based on its sentiments and learn part-of-speech tagging and dense vector for each word. The categorisation of sentiments involves learning core contexts present in the sentences (sequences of words). The part-of-speech tagging divides a sentence into multiple parts-of-speech like an adjective, adverb, conjunctions. It also depends on finding the contexts hidden in the long sequences of words. For the sentiment analysis, [14] achieves an accuracy of $\approx 85\%$ using the recurrent neural network (gated recurrent unit). For the part-of-speech tagging, the accuracy goes up to $\approx 93\%$.

For the clinical data as well, learning long sequences of data proves to be beneficial [16]. In this work, the health states of patients recorded at the different points of time are analysed by accessing their electronic health records (EHR). Using the learned model, the authors predict the future health states of a patient using the sequence of his/her health states in the past. The long-short term memory (LSTM), a kind of recurrent neural network, is used to classify the sequences of health states. An accuracy of $\approx 85\%$ is achieved by applying the necessary regularisation techniques like dropout and weight normalisation.

The research presented in [17, 18] use the recurrent neural networks to model music and speech signals. The authors analyse the performances of the traditional recurrent, long-short term memory (LSTM) and gated recurrent units (GRU). After the analysis, they come to the conclusion that the traditional recurrent units do not

learn semantics present in the sequences, but the LSTM and GRU do. In this study, the sequences of 20 continuous samples (20 steps in time-series of speech) are learned and the next 10 continuous samples (next 10 time steps) are predicted. It is also found out that the GRU performs better than the LSTM in terms of accuracy and running time. For musedata[1], a collection of piano classical music, the performances (average of the negative log-likelihood) on test set noted by the authors are - GRU: 5.99, LSTM: 6.23 and traditional recurrent units: 6.23. They test on 6 different types of musical and speech data and 4 out of these 6 types, GRU works better than the other two units.

These successful approaches benefit from the state-of-the-art sequential learning techniques like the LSTM and GRU recurrent networks. For the Galaxy's scientific workflows, learning the tool connections to predict the next possible tools is inspired by these approaches.

---

[1]`www.musedata.org`

9. Approach

This work proposes to predict a set of next tools at each step of designing a workflow. A learning algorithm is needed which can learn tool connections in a path and predict its next tools. This learning algorithm is a classifier. There are two coveted features of the classifier:

- It should grasp the semantics of tool connections in workflow paths and use them to predict next tools (with an accuracy of $\geq 90\%$).

- Running time and space complexity should be reasonable.

The classifier's running time and space complexity and its accuracy to predict next tools are noted for doing a comparison.

9.1. Steps

Preprocessing is necessary to make workflow paths available for analysis by a classifier. There are multiple steps involved to preprocess them. Figure 25 highlights the sequence of steps. First, all the paths are extracted from workflows and the duplicates are removed. These paths are required by the classifier to understand the dependencies among tools. They are processed by using three different approaches to create smaller paths. Section 9.5.1 describes these approaches in detail. The paths are divided into training and test paths. The classifier consumes the training paths to learn their characteristics along with their next tools. The robustness of learning is verified on the test paths.
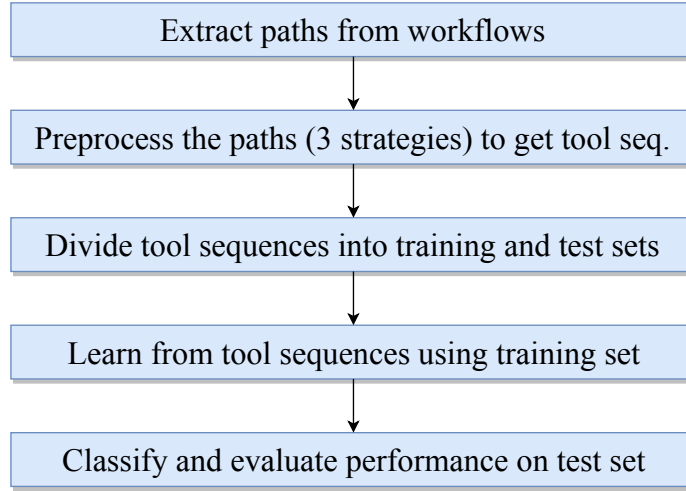
Figure 25.: Sequence of steps to predict next tools in workflows: The flowchart shows a sequence of steps to predict next tools in workflows. They are decomposed into paths. Further, these paths of varying lengths are decomposed to have paths by following three different strategies explained in section 9.5.1. A classifier learns connections from paths in the training set. The learning is evaluated on the test set.

9.2. Actual next tools

Figure 23 shows that a workflow can have more than one path and these paths can share a few tools. Moreover, a path can connect to more than one tool. A classifier needs data in the form of path and its next tools (a tool or a set of different tools).

Path	Tool(s)
Get flanks	AWK
Get flanks > AWK	Intersect
Get flanks > AWK > Intersect	Count, Extract genomic DNA
Get flanks > AWK > Intersect > Count	Bar chart

Table 5.: Decomposition of a workflow: This table shows a few paths and their respective next tools extracted from a workflow shown in figure 23. The next tools of a path are the actual next tools present in the workflow.

A workflow is decomposed into paths. Using the technique explained in table 5, these paths are further decomposed into smaller paths and their respective next tools. This idea is considered because of the necessity of getting predictions in the

same way. It means that when a tool *get flanks* is selected, a classifier should suggest *AWK* as a next possible tool. Again, the tool *AWK* is selected and the sequence becomes *get flanks > AWK*. Given this sequence, the classifier should predict a tool *intersect*. To this sequence, when a tool *intersect* is added, the classifier should predict two tools *count* and *extract genomic DNA* (figure 23). Following this approach of decomposition of paths, paths and their respective next tools are created. The next tools that are assigned to path are its actual next tools. It means that the path is connected to these next tools in workflows.

9.3. Compatible next tools

Tools are connected in a workflow because of their compatible input and output data types. Some can connect only to a few tools, but some can connect to a larger set of tools. All pairs of connected tools are extracted from workflows. Each pair has compatible data types as they are connected. From this set of numerous pairs of tools, a list of compatible next tools is collected for each tool. In a path, *get flanks > AWK > intersect > count > bar chart*, the tool *intersect* connects to *count* tool. It means that these two tools have compatible data types. There are multiple other tools which can connect to *intersect* like *join*, *cut*, *subtract* and many others. These form a compatible set of next tools for *intersect* and can be predicted as next tools for the paths ending in *intersect*. When a classifier predicts next tools for a path and if the last tool of this sequence is compatible with the predicted tools, then the predictions are correct and should be accounted for. These tools are not fed to the classifier for learning but are used only to verify whether the prediction of next tools includes these compatible tools. The number of compatible tools for a tool varies. For example, a tool *concatenate datasets* has ≈ 190 compatible next tools while another tool *mothur dist seqs* has only one compatible next tool.
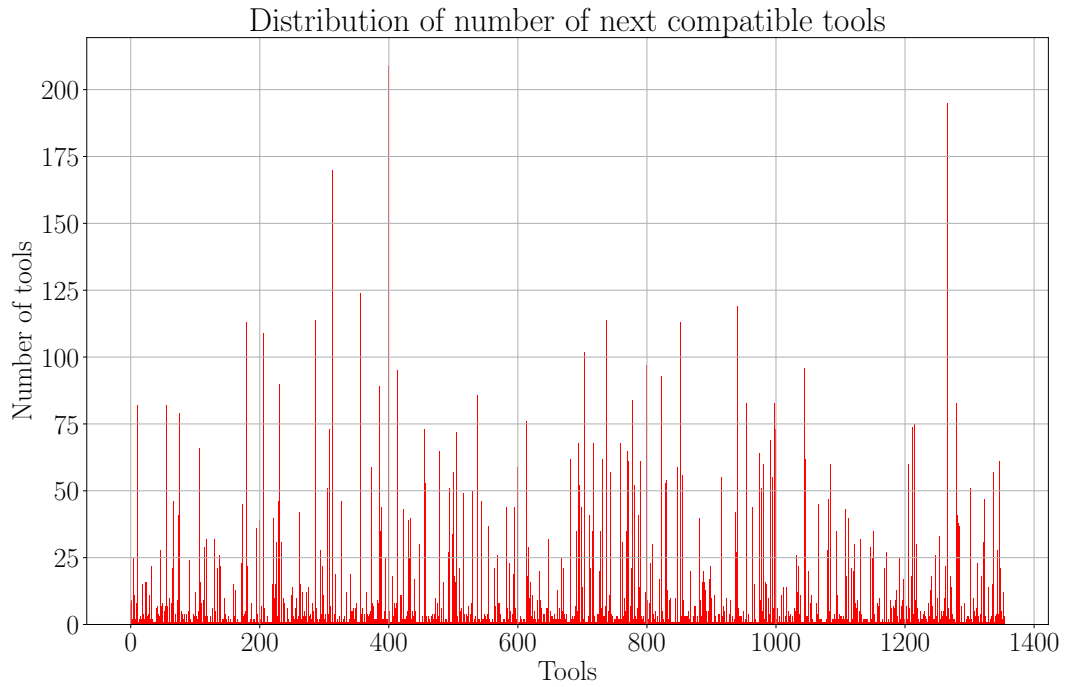
Figure 26.: Distribution of the number of compatible next tools: The bar plot shows a distribution of the number of compatible next tools for each tool. The x-axis shows tools which have at least one compatible next tool. The y-axis shows the number of compatible next tools.

Figure 26 shows a distribution of the number of compatible next tools for each tool. It can be seen that some tools have just one or two next tools while some have a larger number of compatible next tools. This set of compatible next tools is computed from all the workflows analysed in this work.

9.4. Length of workflow paths

The size (number of tools in a path) of paths in workflows varies. A path can be long or short. Figure 27 shows a distribution of the number of tools present in each path. Most of the paths have less than 20 tools while a few contain over 20 tools. It is important to find how the prediction of next tools varies with the sizes of the workflow paths and whether the classifier is sensitive to these sizes.
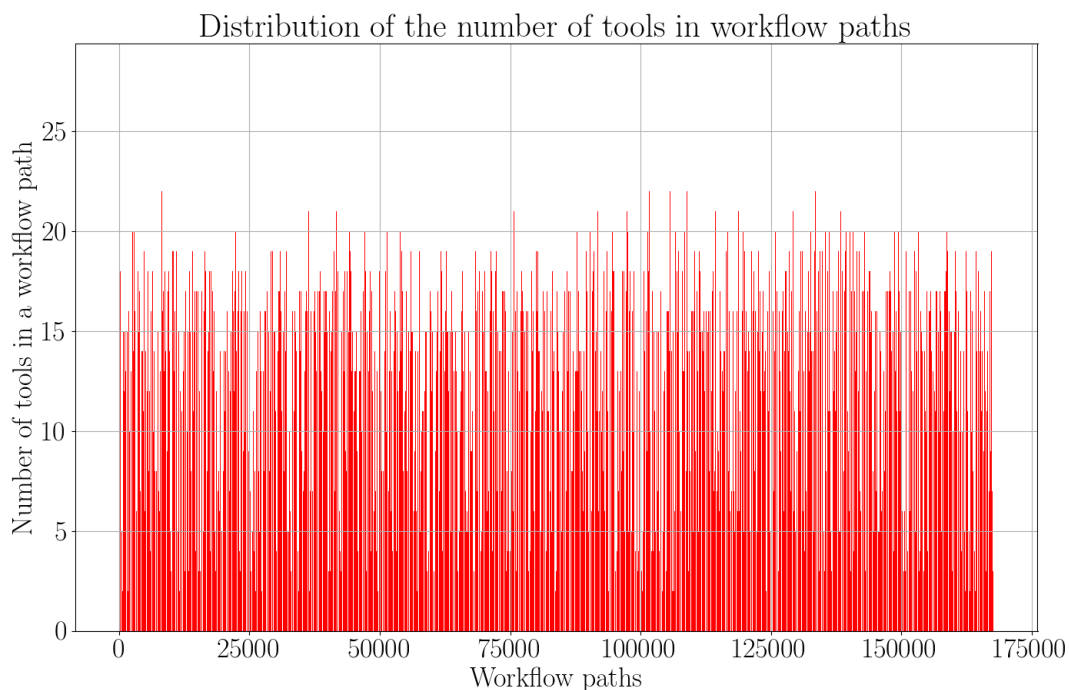
Figure 27.: Distribution of sizes of workflow paths: The plot shows a distri-
bution of the sizes of workflow paths. A workflow path consists of
multiple tools. This distribution shows how many tools are there for
each path. Most of the paths contain less than 20 tools.

9.5. Learning

Figure 25 delineates the steps to predict next tools in workflows. They are decomposed
into paths and then into paths. Each path consists of a set of tools connected one
after another.

9.5.1. Workflow paths

A path enforces a directed flow of information through multiple tools connected in a
series (from left to right). The paths are preprocessed in such a way so that they
can retain their semantics and can be understood by any classifier. Three different
ways of decomposing these paths into tool sequences[1] are used. The decomposed
tool sequences are further divided into training and test paths. The classifier uses

---

[1] *A path and a tool sequence refer to the same entity, a chain of tools, in the thesis. They are used
interchangeably.*

the training paths to learn features. The amount of learning is evaluated on the test paths. It is ensured that the intersection set of the training and test paths is empty. Otherwise, the evaluation of the learned model would be biased [19, 20, 21]. Different methods of the decomposition of paths are discussed in the following sections:

No decomposition

In this approach, paths are used as they are. The last tool of each path is taken as its next tool. A dictionary is created in which these paths are keys and their next tools are values. This dictionary is shuffled and divided into training and test paths. It enforces that no path is present in both the sets of paths. A classifier needs to learn tool connections in these paths and their respective next tools. The learned model is used to predict the last tool of each path in the test set. Figure 28 explains this idea.
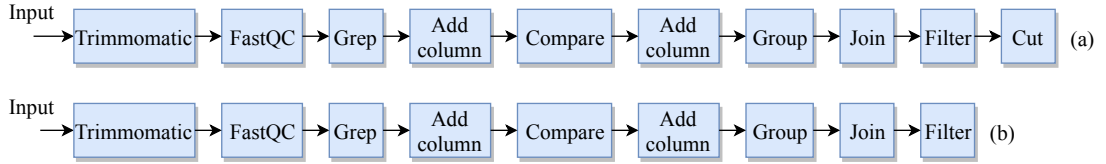
Figure 28.: No path decomposition: The image shows a workflow path. For a path of length n (a), a path of length $n - 1$ (b) is taken out and the last tool is assigned as its next tool. For example, the tool *cut* is a next tool of the previous path.

Decomposition of test paths

In this approach, training paths are used as they are to train a classifier. But, the test paths are decomposed keeping the first tool fixed in each path. Figure 29 shows this decomposition. For a path of length n, $n - 1$ unique paths are created and for each path, the last tool becomes its next tool. A path should contain at least two tools (the second tool is next tool of the first). This decomposition increases the size of test paths. Moreover, it creates a problem of duplication of paths in the training and test paths. A test path is decomposed into smaller tool sequences. Maybe one or more of these tool sequences are present in the training paths. The evaluation would be biased if tool sequences from test paths are present in the training paths. To avoid this situation, the duplicates are removed from the training and test paths before they are fed to the classifier.

Figure 29.: Path decomposition: The image shows how a path is decomposed into smaller tool sequences keeping the first tool fixed. For each tool sequence, the last tool is dependent on all its previous tools (higher-order dependency).

Decomposition of test and train sets

By decomposing paths keeping the first tool fixed, learning task is made easier for a classifier. In the previous section, only the test paths are decomposed. But, in this approach, all the paths are decomposed. The strategy explained in figure 29 is used to obtain a mixture of shorter and longer paths. For this approach as well, a dictionary is created where each key represents a path and its value is a set of next tools. This dictionary is shuffled and divided into training and test paths.

9.5.2. Bayesian networks

A workflow possesses the structure of a directed acyclic graph. Bayesian network is one of the approaches to model this graph. From bayesian network, it is inferred that if the parents of a node are given (in a directed graph), then this node is conditionally independent of all the other nodes which are not its descendants (the set of nodes it

cannot reach through directed edges) [22, 23]. It means that each node in this graph is dependent only on its parents. The structure of workflows can be explained by this model. Bayesian networks can be used to model workflows and the missing values (of nodes) can be predicted. Here, the missing values would be next tools. But, there are a few limitations of this model which are worth considering. The usage of this model involves computing joint probabilities of the nodes in a graph and also the conditional probabilities among them. When the number of nodes increases, it would become hard to keep the computational cost low. Making predictions by learning a probabilistic network is a hard problem [24, 25, 26]. Due to these reasons, the bayesian network is not used in this work for predicting next tools in workflows.

9.5.3. Recurrent networks

A workflow may have multiple paths and they can share a few tools. These paths are extracted from the workflows and the duplicates are removed. They are assumed to be independent of one another which keeps the analysis simple yet powerful. In a path, each tool is dependent on all its parents (previous tools in the path). This relation is called higher-order dependency [27]. It is important to learn these higher-order dependencies in order to be able to predict next tools for path. Figure 30 shows these dependencies for a path. The tool *text reformatting* is not the only cause of tool *sort* but tools *datamash* and *concatenate datasets* as well. A classifier should model these dependencies for variable length paths.
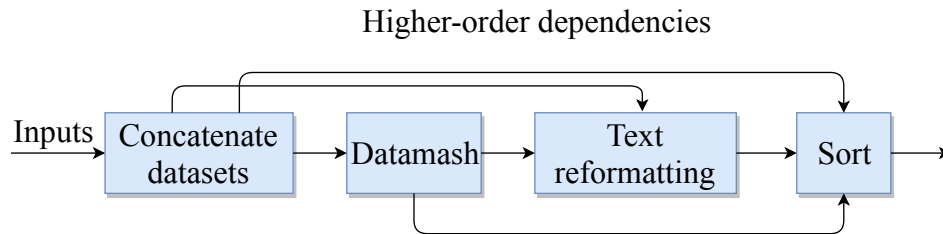
Figure 30.: Higher-order dependency: The image shows a small path where four tools are arranged in a sequential manner. Each tool depends not only on its immediate parent tool, but all the previous tools in a path.

The recurrent neural network is a natural choice for the classifier which can learn these dependencies in workflow paths. To model these dependencies, the network keeps a hidden state at each step of processing paths. It combines information from previous tools and the current tool. It is computed as:

$$h_t = \phi(h_{t-1}, x_t) \tag{31}$$

where h_t is the hidden state at step (or time) t, h_{t-1} and x_t are the hidden state at the previous step $(t-1)$ and input at t respectively. ϕ is a nonlinear function.

More formally, the equation 31 is written as:

$$h_t = g(W_{input} \times x_t + U_{recurrent} \times h_{t-1}) \tag{32}$$

where W_{input} and $U_{recurrent}$ are the weight matrices for the input and recurrent units respectively. The hidden state keeps information about the previous steps. At each step, x_t is an input. $g()$ is a bounded, nonlinear function like *sigmoid* (equation 39). The joint probability of all these input variables (x_i) is given by:

$$p(x_1, x_2, ..., x_T) = \prod_{t=1}^{T} p(x_t | x_{t-1}, ..., x_1) \tag{33}$$

where x_t is the input at step t, $p(.)$ is the probability distribution and T is the length of a path (total time-steps). From equation 33, the input at step t is reliant on the previous inputs in a sequence. To predict next input (or next tool in a path), this conditional probability distribution should be captured using the hidden state (h_t) [17, 28].

In equation 32, there are two matrices one each for the recurrent units and inputs respectively. Learning higher-order dependencies depends on the gradients of errors with respect to the parameters (recurrent and input weight matrices). The gradient at a step is the product of gradients from all previous steps. If the gradients are small which inherently means that the recurrent units are not capturing higher-order dependencies, then the gradient can quickly slip towards zero and disappear (the product of small numbers would be small). In another scenario when the gradients are large, the product can easily explode to become a large number. Both these situations are collectively known as vanishing/exploding gradients problem. The traditional recurrent units are prone to show this behaviour [29]. In order to avoid these situations which can hamper learning, two variants of recurrent units are proposed:

- Long-short term memory units (LSTM) [30]

- Gated recurrent units (GRU) [28]

In this work, the gated recurrent units (GRU) is explored which is recently proposed and is simpler than the LSTM and contains fewer parameters. The performance of these two variants is comparable [17].

Gated recurrent units (GRU)

The GRU has gates which control the flow of information (figure 31). The reset gate r checks how much information from the previous time steps should be carried forward. If it is 0, then all the information from the previous time steps is discarded. If it is 1, all the information accumulated over the previous time steps is taken forward. The update gate controls how much of the unit's own information would be used when computing the current memory content.
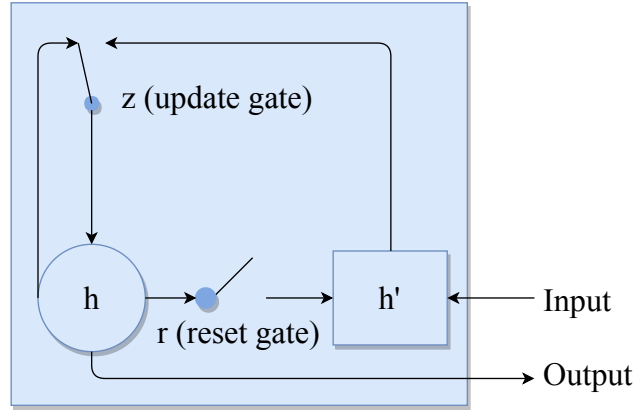
Figure 31.: Gated recurrent unit: The image shows a gated recurrent unit with two gates, r as a reset gate and z as an update gate. The activation of the GRU is h and the proposed activation is h' [17].

$$h_t = (1 - z_t) \times h_{t-1} + z_t \times h_t'$$ (34)

where h_t and h_{t-1} are the current and previous step activations respectively, z_t is the value of update gate and h_t' is the current proposed activation. The update gate is calculated using the following equation:

$$z_t = \sigma(W_z \times x_t + U_z \times h_{t-1})$$ (35)

where $\sigma(.)$ is the *sigmoid* function and W and U are the input and recurrent weight matrices respectively. The current proposed activation (in equation 34) is

computed using:

$$h'_t = \tanh(W \times x_t + U \times (r_t \odot h_{t-1})) \tag{36}$$

where h'_t is the proposed current activation, W and U are the input and recurrent weights matrices, r_t is the value of the reset gate and h_{t-1} is the previous step activation. The symbol $\odot$ is an element-wise multiplication between r_t and h_{t-1}. The *tanh* is an activation function and is given as:

$$f(x) = \frac{e^x - e^{-x}}{e^x + e^{-x}} \tag{37}$$

The reset gate is given as:

$$r_t = \sigma(W_r \times x_t + U_r \times h_{t-1}) \tag{38}$$

where r_t is reset gate which controls how much information from the previous activation should be used at step t. W_r and U_r are the input and recurrent weights matrices respectively. x_t is the current input at step t and h_{t-1} is previous step activation. An important point to note here is that an output does not only depend on current input but on previous inputs as well (equation 34). A memory of previous inputs is maintained. It enables the gated recurrent units network to extract latent features present in long sequences that lead to a specific output.

9.6. Pattern of predictions

The classifier is designed to generate a probabilistic prediction of next tools for all paths. There are n unique tools which are used to create workflows. The classifier should assign a score to each tool of being the next tool of a path. The dimensionality of the output should be n.

9.7. The classifier

The recurrent neural network is used to classify paths and predict next tools. This network contains several layers and they are arranged as a stack. The first layer consumes paths and the last layer gives predictions. The hidden recurrent layers do all the computations required to do the classification of paths. While classifying, the paths are mapped to their respective next tools. Figure 32 shows how the classifier assigns scores to tools of being the next tool of a path.
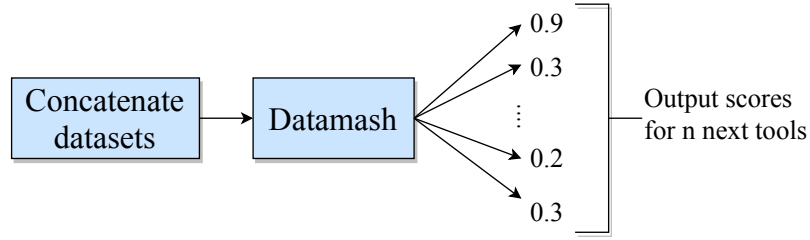
Figure 32.: Predicted scores for next tools: The image shows how the scores are assigned by the classifier to a set of n tools. The scores vary between zero and one. Each score contains an importance of each tool to become the next tool of a path. In the example, there are two tools in the path and the predicted scores of next tools are given. The predicted scores are sorted in descending order and a few top tools are selected.

9.7.1. Embedding layer

The first layer of the recurrent neural network is an embedding layer. It learns a dense, fixed-length vector for each tool (figure 34e). An index (an integer) is assigned to each tool and it is converted to an embedding vector. It represents features associated with that tool. It means that an embedding vector for a tool encodes the information of the context in which the tool is being used. The tools which are used in similar context, their embedding vectors are similar.

9.7.2. Recurrent layer

Two hidden recurrent layers containing gated recurrent units are used. These layers are responsible for doing the computations given in equations 34-38. The hidden layers are stacked one upon another and they contain an equal number of gated recurrent units. The stacking of layers learns deeper features in paths. The hidden states of units in the first layer become the inputs to the units of the next hidden recurrent layer. Figure 33 shows these recurrent layers.

9.7.3. Output layer

An output is computed from the output (last) layer of the recurrent neural network. It is a dense layer having the same dimensionality as the number of tools. Each dimension holds a real number between zero and one which is a score assigned to a tool of being the next tool for any path. The *sigmoid* function (equation 39) is used as an activation for this layer:
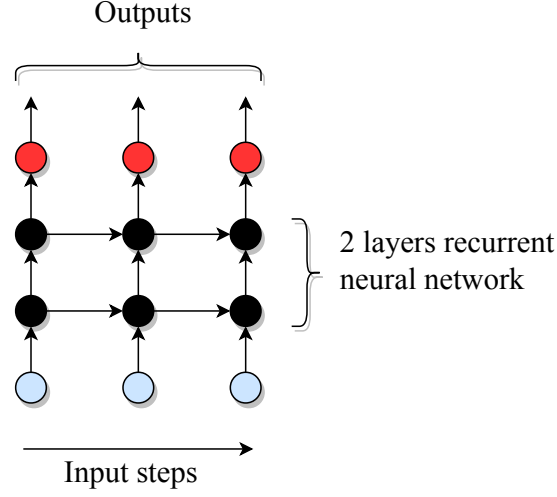
Figure 33.: Recurrent neural network: The image shows the stacked gated recurrent units layers and how they pass information from the input layer to the output. The output of the first recurrent layer is used as an input to the next recurrent layer. The blue circles denote the input steps (different tools in a path), the black ones form the two recurrent layers and the red circles form the output layer [31].

$$f(x) = \frac{1}{1 + e^{-x}} \tag{39}$$

9.7.4. Activations

An activation is a function which transforms the input of a neuron (a node in a neural network) to an output. It can either be linear or nonlinear. There are multiple activation functions like *softmax, sigmoid, tanh, relu, linear* and many more[2]. It is chosen based on the kind of output required for the further evaluation. The output of a neuron is given by:

$$y^j = \phi(\sum_{i=1}^{n} w_i \times x_i + b)^j \tag{40}$$

where y is an output of the neuron j, w_i is the weight of the ith input connection to the neuron j, x_i is an input and b is bias for neuron j. ϕ is an activation function. The *sigmoid* is used as an output activation because the next tools are independent of one another and it learns the output of each tool separately. The *softmax* activation

---

[2]https://keras.io/activations/

can replace it, but it normalises the exponents of outputs which is undesired. The *sigmoid* assigns a real number between zero and one to each tool at the output layer. Another activation is exponential linear unit (*elu*). It is used as an activation for the recurrent layers. In equation 36, *tanh* is replaced by *elu* activation. It is given by:

$$f(x) = \begin{cases} x, & \text{if } x > 0 \\ \alpha \times (e^x - 1), & \text{if } x \leq 0 \end{cases}$$

It has a special feature of being negative when an input is negative. This feature allows mean activation (output) to get closer to zero compared to other activation functions like *relu* which is always positive. As mean activations get closer to zero, the approximated and actual gradients become closer to each other. Due to this, the learning becomes faster and increased drop in error is achieved [32].

9.7.5. Regularisation

Overfitting is a common phenomenon in the field of machine learning. It occurs when a classifier starts memorising training data without learning general features present in data. It leads to an increased learning on the training data but no learning on test data. The error on the train data decreases but the error on the test data either stops decreasing or sometimes increases. The classifier stops generalising and would predict new data with an increased uncertainty. A variant of a neural network is used in this work for the classification task. It is prone to overfitting as it tends to derive a complex model. If the size of the training data is not enough, it starts overfitting. To generate a model which learns general features, it is important to apply measures to remove or reduce overfitting. The regularisation is a technique to overcome this common problem. There are many techniques to regularise a neural network like dropping out random units (dropout) and decaying weights to stop them from becoming large. In this work, dropout is used as a regularisation method to tackle overfitting [33].

Dropout

Dropout removes connections momentarily from a neural network and thereby changing the network structure during each weight update. It randomly sets the output of some connections to zero and due to this, the network behaves in a novel manner. The network becomes less powerful and it stops picking bias from training

data. A real number between zero and one is specified as dropout which is the percentage of neurons to be dropped. The dropout is applied to the input, output and recurrent connections of the recurrent neural network. The embedding layer also has a dropout layer for its output. The amount of dropout is a hyperparameter and a suitable value should be found out for which the drop in training and validation losses remains stable and close to each other [34, 35]. Moreover, the amount of dropout depends on the complexity of a neural network and the amount of data.

9.7.6. Optimiser

An optimiser is used to minimise error computed by an error function. Mini-batch *RMSProp* optimiser is used to find optimal weights (for features) which minimise error. *RMSProp* is a variant of stochastic gradient descent with an adaptive strategy for learning rate [36]. It adapts learning rate according to gradients. It keeps a track of the previous gradients and updates the learning rate by dividing with an average of the square of the previous gradients. The weight update is given by the following equations:

$$MeanSquare(w,t) = 0.9 \times MeanSquare(w, t-1) + 0.1 \times \frac{\partial E}{\partial w}(t) \qquad (41)$$

$$w_{t+1} = w_t - \frac{\eta}{\sqrt{MeanSquare(w,t)}} \times \frac{\partial E}{\partial w}(t) \qquad (42)$$

where $MeanSquare(w,t)$ is the mean of squared gradients until time t, $\frac{\partial E}{\partial w}$ is a partial derivative (gradient) of the error function with a parameter w at time t and η is learning rate.

Learning rate

Learning rate is an important parameter for an optimiser which determines the amount of update at each time step. If the learning rate is high, there is a risk of an optimiser divergence. Instead of going to the minimum of error surface, which is the expected behaviour, the optimiser keeps oscillating on the error surface and bypassing the minimum. On the other hand, if the learning rate is low, the minimum may never be reached as learning steps become too small. The optimiser does not converge to the minimum or take a large amount of time to converge. Due to these reasons, setting a good learning rate is a key to converge in a reasonable amount of

time.

Loss function

Binary cross-entropy[3] is used as a loss function for the *RMSProp* optimiser. It is well-suited for multilabel classification. It is a kind of classification of data with multiple outputs. For this work, a path can connect to more than one tool and due to this, there can be multiple next tools for a path. Therefore, multilabel classification is needed for this work. The loss function is given by:

$$loss_{mean} = -\frac{1}{N}(\sum_{i=1}^{N} y_i \times log(p_i) + (1 - y_i) \times log(1 - p_i)) \tag{43}$$

where N is the dimension of output layer (total number of next tool positions), y is actual next tool vector and contains either zero or one, p is predicted next tool vector. The predicted next tool vector p contains real numbers between zero and one. The mean loss is a small number when the actual and predicted next tool vectors are comparable. In equation 43, the summation is always negative or zero making the mean loss to be always positive or zero.

9.7.7. Precision

Precision is computed for each path at the end of each training epoch. All the predicted next tools are matched either with actual or compatible next tools for a path and the correctly predicted next tools are computed. It is averaged over all the paths in test paths to get an average precision for a training epoch.

---

[3]`https://github.com/keras-team/keras/blob/master/keras/backend/tensorflow_`
`backend.py`

10. Experiments

Workflows are collected from the Galaxy's main[1] and Freiburg servers[2]. There are $\approx 900,000$ paths in these workflows. Out of all these paths, $\approx 167,000$ paths are unique. The duplicate paths are removed. A recurrent neural network (GRU) is trained on training paths (80% of all paths) and evaluated on test paths (20% of all paths). A small part of the training paths (20%) is reserved as validation paths. It is used to find the correct values of multiple parameters of the recurrent neural network. The loss is also computed on these validation paths. The *bwForCluster*[3] provides computing resources for preprocessing the workflows and training and evaluating the recurrent neural network.

10.1. Decomposition of paths

The paths are decomposed by following the approaches explained in section 9.5.1. The performance is measured separately for each approach. In the first approach, no path is decomposed and the recurrent neural network is trained and tested on actual paths. In the second approach, only test paths are decomposed as described in figure 29 and the recurrent neural network is trained on actual paths. In the last approach, both the training and test paths are decomposed as described in figure 29. The recurrent neural network is trained using a mixture of smaller and longer paths. The configuration of the recurrent neural network is kept same for all the three approaches.

10.2. Dictionary of tools

Tool names present in paths cannot be used by any classifier. They need to be converted into numbers. To do that, a dictionary is created where each tool name is

---

[1] https://usegalaxy.org/
[2] https://usegalaxy.eu/
[3] https://www.bwhpc-c5.de/wiki/index.php/Main_Page

assigned an integer. The tool names are replaced by their respective indices from the dictionary and each path becomes a sequence of integers (figure 34a and 34c). In addition, a reverse dictionary is also created to replace any index by its name.

10.3. Padding with zeros

Training, test and validation paths have variable sizes. Some of these paths are short while some are long. But, the recurrent neural network can take only a fixed-size sequence. To deal with this issue, the maximum path length (number of tools) is set to 25 which captures all the paths. Figure 27 shows that the number of tools in each path is less than 25. For shorter paths, a padding of zeros is added in the beginning to ensure that all paths have the same length. Moreover, it is undesirable that the recurrent neural network learns any feature from these padded zeros. To avoid this, a flag is set (in the implementation of the embedding layer) to mask[4] these streams of zeros. Due to this, the recurrent neural network considers only the useful indices in a path. As zero is chosen for the padding, it does not represent any tool in the dictionary.

Figure 34 shows that how a path and its possible next tools are transformed into their respective vectors. These vectors (34d and 34e) are used by the recurrent neural network for training and evaluation. Figure 34a shows a path with three tools arranged in an order as it would appear in any workflow. Figure 34b shows next tools for the path. The section 10.2 explains that each tool is represented by an integer and is shown in figure 34c. The length of the vector in 34c is 25. The padding of zeros is also shown followed by the corresponding indices of tools (figure 34c). In each vector, the padding of zeros precedes the sequence of tool indices. Each index is further transformed into a fixed-length vector (embedding) as shown in figure 34e. The length of this embedding vector remains the same for all the tools and is defined by the size of the embedding layer (512). 512 dimensional vector is learned for each tool's index and arranged as shown in figure 34e. The order of the tools is maintained as present in the original path in figure 34a. Figure 34d shows how the next tools vector is arranged. A vector of zeros with the size equal to the number of tools is taken. The corresponding indices of the next tools are set to one in this vector. For example, *addvalue* tool has an index 4 in the dictionary. Therefore, the fourth position of the next tool vector is set to one (figure 34d). This is repeated for all the

---

[4]https://keras.io/layers/embeddings/

next tools for a path. Figure 34d contains two positions set to one representing the next tools for the path in figure 34a.

Tool sequence | Possible next tools of the tool sequence

Trimmomatic > FastQC > Grep | AddValue, Datamash transpose
(a) | (b)

[0, 0, 0, ..., 12, 7, 80] | [0, 0, 0, 1, ..., 0, 0, 0, 1, 0, 0, 0]
(c) | (d)

[0, 0, 0, ..., [0.1, 0.2, ... , 0.09], [-0.2, 0.8, ..., 0.03], [0.34, 0.5, ..., 0.06]]
(e)
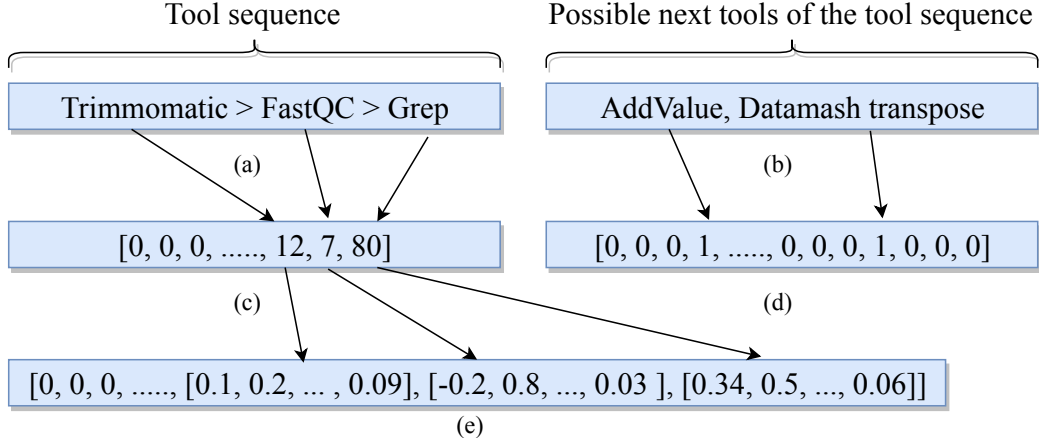
Figure 34.: Vectors of path and its next tool: The image shows how vectors are created for a path and its next tools in order to make them available for the recurrent neural network. Figure 34a shows a path with three tools. 34b shows its next tools. Figure 34c shows the arrangement of padding of zeros along with the indices of tools in a fixed-length vector (25). Figure 34d shows how next tools vector is arranged. The corresponding positions of next tools are set to one and the rest of the positions are set to zero. In figure 34e, each index belonging to a tool is transformed into a fixed-length embedding vector. This is done by the embedding layer of the recurrent neural network. The size of the embedding layer defines the length of this embedding vector.

10.4. Network configuration

The gated recurrent unit, a variant of the recurrent neural networks, is used as the classifier. The recurrent neural network has several layers and many hyperparameters. An embedding layer is used as an input layer which learns a fixed-size vector (512) for each index belonging to a tool. The number of unique tools in all the workflows is 1,800. As the number of tools increases, it is important to increase the size of embedding layer. The dropout is applied to the output of this layer in order to reduce overfitting. Two hidden recurrent layers with the gated recurrent units are used to model the paths. Each layer has a fixed number of memory units. The number of memory units specifies the dimension of the hidden state (equation 34). Dropout is applied to the inputs, outputs and recurrent connections for each hidden recurrent

layer. The amount of dropout remains the same everywhere in the recurrent neural network. The last layer is a dense layer and has a size equal to the number of tools. This is because, for each path, the recurrent neural network generates scores for all the tools to be the next tool of a path. The tools having higher scores at the output layer possess higher probability of being the next tools.

10.4.1. Mini-batch learning

In mini-batch learning, a smaller set from training paths is chosen to update the weights. Multiple candidate values (batch size) like 64, 128, 256 and 512 are chosen to see the effect on the loss and precision while keeping all other parameters fixed. Its value is set to 512 for the baseline network. The recurrent neural network is allowed to learn on training paths over multiple epochs. An epoch consists of multiple iterations and in each epoch, all the training paths are used. In each iteration, 512 paths are used to approximate the weight update. If there are 2560 (512×5) training paths, then 5 iterations will make one epoch with 512 as batch size. The recurrent neural network is sensitive to this number as a small number can add a lot of noise to the weight update [37].

10.4.2. Dropout

For setting dropout, different numbers are used to find the best with the recurrent neural network and training paths. The values like 0.0 (no dropout), 0.1, 0.2, 0.3 and 0.4 are used while keeping all other parameters fixed. The loss on validation paths is a key indicator of overfitting.

10.4.3. Optimiser

A few optimisers like the *stochastic gradient descent (SGD)*, *adam*, *rmsprop* and *adagrad* are used to find which one provides a stable learning and enables the recurrent neural network to achieve the best precision. All the other parameters are kept fixed. They all minimise the cross-entropy loss between actual and predicted next tools. The default configurations of these optimisers are used as set by the keras library[5].

---

[5]`https://github.com/keras-team/keras/blob/master/keras/optimizers.py#L209`

10.4.4. Learning rate

Different learning rates are used to find a stable learning pattern by the recurrent neural network. They range from 0.0001, 0.005, 0.001 and 0.01. A smaller learning rate tends to slow down the convergence of the optimiser while a higher rate can diverge it. It is important to avoid both the situations to ensure a stable learning. All other parameters are kept fixed.

10.4.5. Activations

There are multiple choices of activation functions like *tanh*, *sigmoid*, *relu* and *elu*. *tanh* is the default activation[6] while *elu* is one of the recently proposed activations. All other parameters are kept fixed.

10.4.6. Number of recurrent units

The hidden recurrent layers need memory units (dimensionality of hidden state) to learn from the workflow paths. To choose a size which expresses the hidden states to ensure better learning, several sizes like 64, 128, 256 and 512 are used one by one. All other parameters are kept fixed.

10.4.7. Dimension of embedding layer

This dimension specifies the length of the dense vectors learned for each tool. Various sizes like 64, 128, 256, 512 and 1024 are used to see the effect on the precision and loss. All other parameters are kept fixed.

10.5. Accuracy

The classifier's accuracy is reported as precision on test paths over multiple epochs of learning on training paths. The learning saturates and training and validation losses do not decrease anymore after 40 epochs. It means no more learning is possible and training should be stopped. The learned model saved for the last epoch is used for making the predictions of test paths.

---

[6]`https://keras.io/layers/recurrent/#gru`

11. Results and analysis

In this section, the performance of the recurrent neural network is visualised and discussed for three different approaches of decomposition of paths (section 9.5.1). Different values of various parameters like optimiser, learning rate, activation, batch size, number of memory units, dropout, embedding dimension and length of paths are used and their performances are compared. The top-1 and top-2 accuracies are also compared. A slightly different neural network with only dense layers is also used to show a performance comparison with the recurrent neural network. The values of the parameters used by the recurrent neural network are as follows:

- Number of epochs is 40

- Batch size is 512

- Dropout is 0.2

- Number of memory units is 512

- Dimension of embedding layer is 512

- Maximum length of paths 25

- Test set is 20% of the complete set of paths

- Validation set is 20% of the training set

- Activation is *elu*

- Output activation is sigmoid

- Loss function is binary cross-entropy

These parameters remain the same for all three approaches and define a baseline configuration of the recurrent neural network. By experimenting with the different values of these parameters, the possibilities are explored to improve performance.

11.1. Notes on plots

For the plots in figures 35-44 and 47, there are few common points to note:

- The x-axis shows the number of training epochs. For subplots (a) and (b), the y-axis shows an average precision and for subplots (c) and (d), the y-axis shows cross-entropy loss.

- The subplot (a) shows absolute precision. If a path has five actual next tools, top five predicted next tools are taken out from using predicted model. If out of the five predicted next tools, only four of them match with the actual next tools, then the absolute precision for this path is $\frac{4}{5}$. The average precision is computed over the test paths after each epoch.

- The subplot (b) shows compatible precision. While computing absolute precision, some false positives (wrong next tools) are also predicted which are not present in the actual next tools for a path. In this case, these false positives are matched with the compatible set of tools belonging to the last tool of the path. If some or all of the false positives are present in this compatible set, then they add up to absolute precision to give compatible precision. For example, in the last point, there is one false positive out of the five predicted next tools. This false positive is checked in the compatible set of the last tool of path. If it is present, then compatible precision becomes 1.0. If not, it stays equal to the absolute precision ($\frac{4}{5}$). The compatible precision is at least as good as the absolute precision.

- The subplot (c) shows the cross-entropy loss on training paths. It is computed by the recurrent neural network as shown in equation 43.

- The subplot (d) shows the cross-entropy loss on validation paths. The last 20% of training paths are the validation paths. The loss is computed by the recurrent neural network after training on the first 80% of training paths.

11.2. Performances of different approaches of path decomposition

11.2.1. Decomposition of only test paths

In this approach, the paths in the test set are decomposed keeping the first tool fixed as explained in figure 29. The training paths are kept as such. The results are shown in figure 35. The idea is to make the recurrent neural network learn tools connections using longer paths and predict next tools for shorter paths. It models a real application of the work - learning longer paths and predicting shorter paths. But, as the result suggests, the learning does not happen as desired. Absolute precision is worse than compatible precision. The absolute precision is $\approx 22\%$ while the compatible precision measures $\approx 43\%$ (figures 35a and 35b) at the end of training. However, the cross-entropy loss for validation paths drops in a steady manner and saturates (figures 35c and 35d). The learning happens but only for the training paths (longer paths) and not for the test paths (shorter paths) as the precision is low. The overall training and evaluation time was ≈ 28 hours. Each epoch took ≈ 20 minutes for training. The number of training paths was $\approx 96,000$ while the number of test paths was $\approx 62,000$. But, only half of the test paths ($\approx 31,000$) were used for evaluating the trained model.
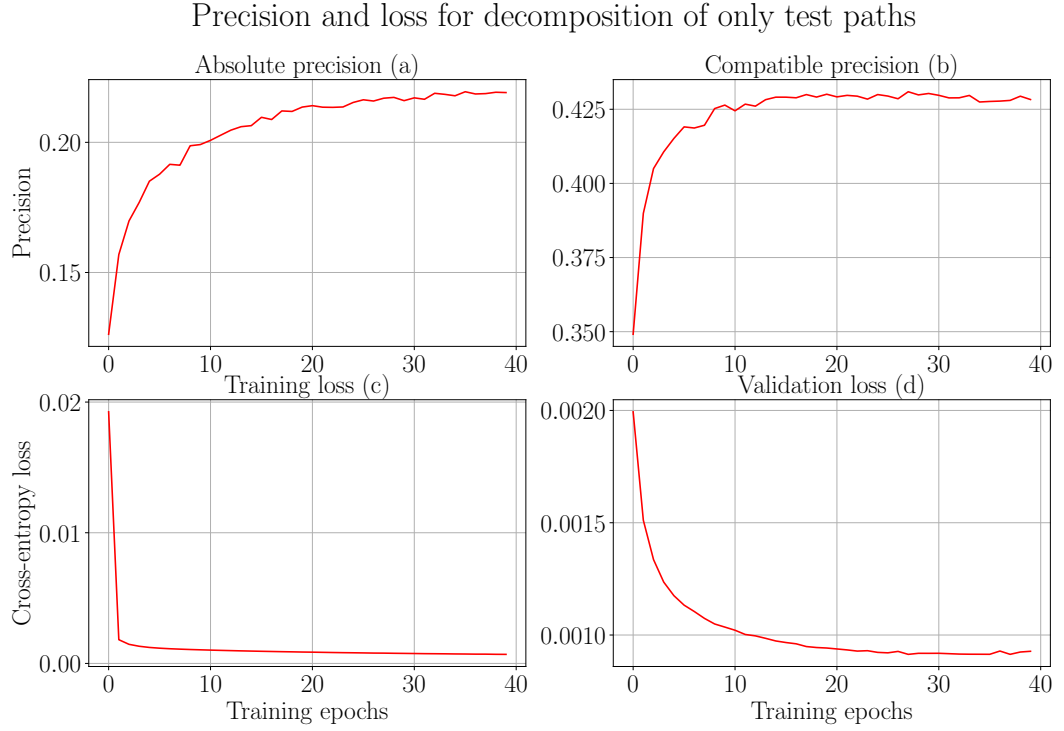
Precision and loss for decomposition of only test paths

Figure 35.: Performance of the decomposition of only test paths: The plot shows classification performance of an approach where only test paths are decomposed keeping the first tool fixed. The training paths are kept as such. The idea is to train a recurrent neural network on longer paths and test on shorter paths. The subplots (a) and (b) show precision while (c) and (d) show the cross-entropy loss change over multiple epochs of training.

11.2.2. No decomposition of paths

In this approach, the paths from the workflows as used as such for both, the training and test paths. The recurrent neural network is made to learn and evaluate on longer paths. The last tool in each of these paths is used as the next tool. The results in figure 36 are encouraging. The subplot 36a reaches a precision of $\approx 89\%$ at the end of training. The compatible precision is $\approx 98\%$ and is much better than the previous approach. The validation loss (figure 36d) drop is steady and comparable to the training loss (figure 36c). The overall training and evaluation time was ≈ 22 hours. Each epoch took ≈ 20 minutes for training which is same as the previous approach because the number of training paths remains almost same. It took less time compared to the previous approach because of the smaller size of test paths.

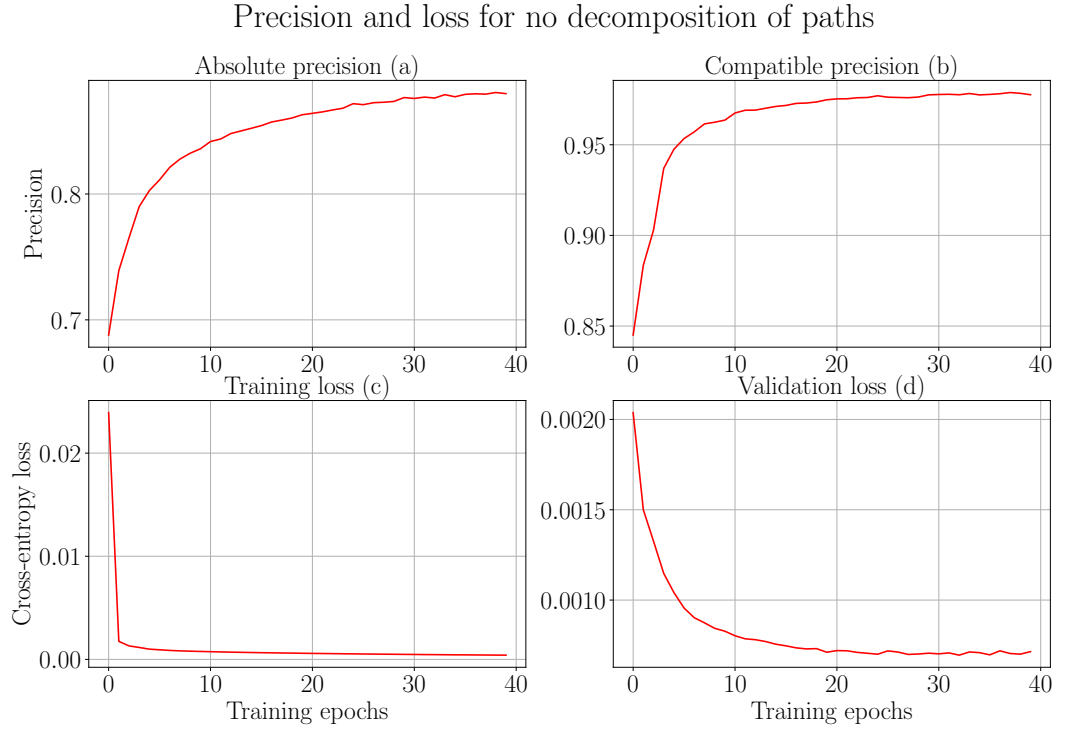The number of training paths was $\approx 90,000$ while the number of test paths was $\approx 22,000$.

Precision and loss for no decomposition of paths

Figure 36.: **Performance of no decomposition of paths**: The plot shows classification performance of an approach where no paths are decomposed. The idea is to train and test the recurrent neural network on longer paths. The subplots (a) and (b) show precision while (c) and (d) show the cross-entropy loss change over multiple epochs of training.

11.2.3. Decomposition of train and test paths

All the paths are decomposed keeping the first tool fixed. The idea here is to make the recurrent neural network learn and predict on shorter as well as longer paths. The results are shown in figure 37. Absolute precision is $\approx 89\%$ while compatible precision is $\approx 99\%$. The results are comparable to the previous approach. To create a workflow, a tool is chosen and its next tools are predicted. Again, one more tool is added to the previous tool and using these two connected tools, the next tools are predicted and so on. Therefore, this approach is more practical than the previous approach. The paths are decomposed to have many shorter paths. Due to this, size of the training paths increases which means that more training time is required.

The training along with the evaluation of the test paths finished in $\approx$ 48 hours. The training for each epoch took $\approx$ 45 minutes. The number of training paths was $\approx 168,000$ while the number of test paths was $\approx 42,000$.

Precision and loss for decomposition of train and test paths
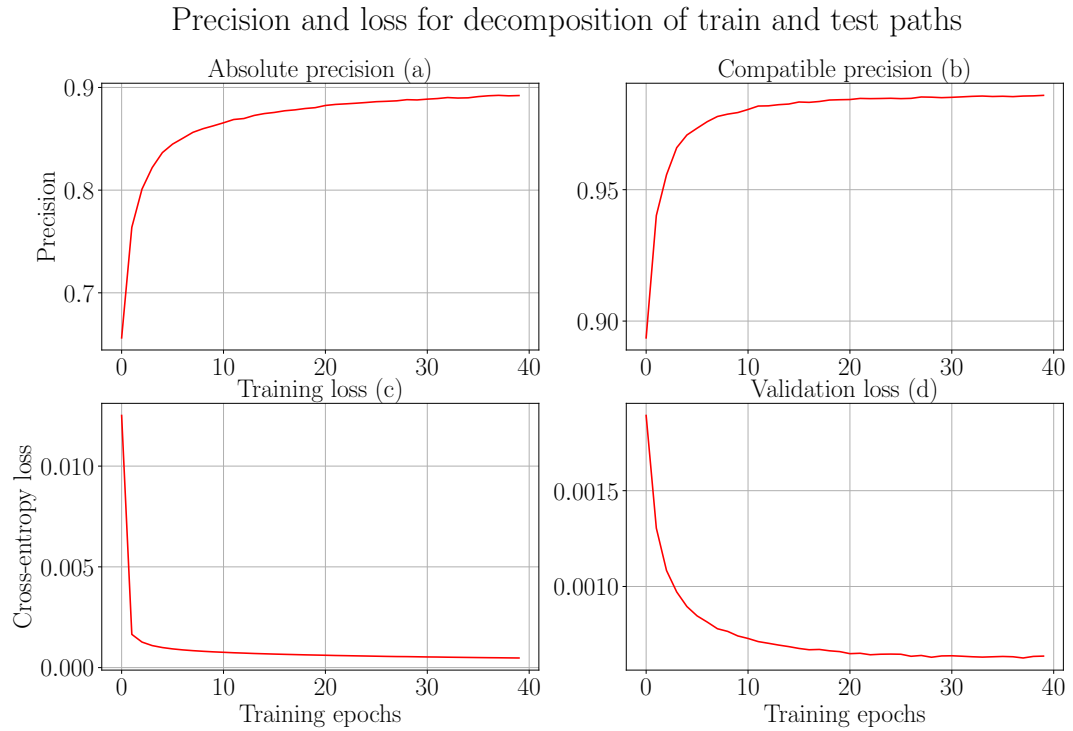
Figure 37.: Performance of the decomposition of all paths: The plot shows classification performance for an approach where all the paths are decomposed keeping the first tool fixed. The idea is to make the recurrent neural network learn and predict on the shorter as well as longer paths. The subplots (a) and (b) show precision while (c) and (d) show the cross-entropy loss change over multiple epochs of training.

11.3. Performance evaluation on different parameters

The recurrent neural network has many parameters and they need to be tuned to the amount of data and to each other so that it learns and predicts in a reliable way. Their right combination is needed to attain a reasonable accuracy and to avoid too much learning (overfitting) and too less learning (underfitting). These parameters include optimiser, learning rate, activation, batch size, number of recurrent (memory) units,

dropout and dimension of embedding layer. There are a few more metrics on which the evaluation is done. These include top-k accuracy and length of paths. A deep network with only dense layers is also used as a classifier to compare classification performance with the recurrent neural network.

11.3.1. Optimiser

Four optimisers are used to find out which one works best. Optimiser like *stochastic gradient descent (SGD)* [36], *adaptive sub-gradient (adagrad)* [36], *adam* [38] and *root mean square propagation (RMSProp)* [36] are used for the analysis. All other parameters are kept constant. From figure 38, it is concluded that the SGD performs worst on both the metrics, precision and loss. The absolute and compatible precision do not improve and the drop in loss curve starts very late during training. The SGD starts off with a high loss value (0.65) and does not drop much within the 40 epochs of training. Out of the remaining three optimisers, *RMSProp* performs best. The performance of *adam* is comparable to *RMSProp*. The adam optimiser catches up with the precision measured by the *RMSProp*, but slowly. Their performances converge later in the training. The plot shows that the choice of the *RMSProp* as an optimiser for the baseline network is beneficial for learning. In general, *RMSProp* is a good choice for the recurrent neural networks [39]. The bad performance of the SGD may be attributed to its non-adaptive parameter update method. The update of parameters does not adapt to the gradients which is an important feature in the adaptive optimisers (*RMSProp* and *adam*). The adaptive optimisers adjust the parameter update with the gradients of the previous steps.
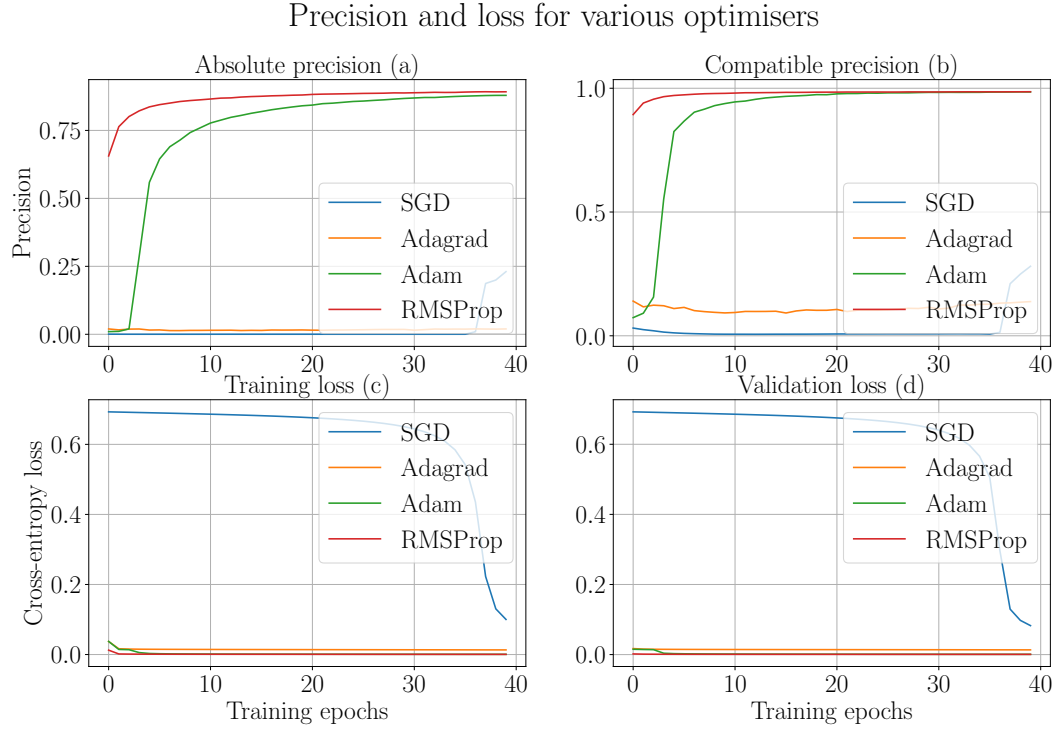
Figure 38.: Performance of different optimisers: The plot shows the performance of different optimisers. The subplots (a) and (b) show precision while (c) and (d) show the cross-entropy loss change over multiple epochs of training. The four optimisers are the *stochastic gradient descent (SGD)*, *adaptive sub-gradient (adagrad)*, *adam* and *root mean square propagation (RMSProp)*. All other parameters of the network are kept constant.

11.3.2. Learning rate

Multiple values of learning rate from small (0.0001) to high (0.01) are used to ascertain their effect on learning. The performance obtained by using these different learning rates while keeping other parameters constant is shown in figure 39. Higher learning rate (0.01) diverges the optimiser as precision drops during training. The training loss increases and its curve has sharp edges. For the validation loss as well, there is no stable pattern (continuous drop). These situations are undesirable and they inform that the learning rate should be kept smaller. A smaller value of 0.005 works better than the previous one but not completely because the precision drops slightly towards the end of training. The smaller values 0.001 and 0.0001 help in learning as the precision improves and the loss drops during entire learning in a

steady way. 0.0001 ensures good learning but it is slower and would need more epochs (and more time) to converge. 0.001 works best out of all these values on both the metrics.

Precision and loss for various learning rates
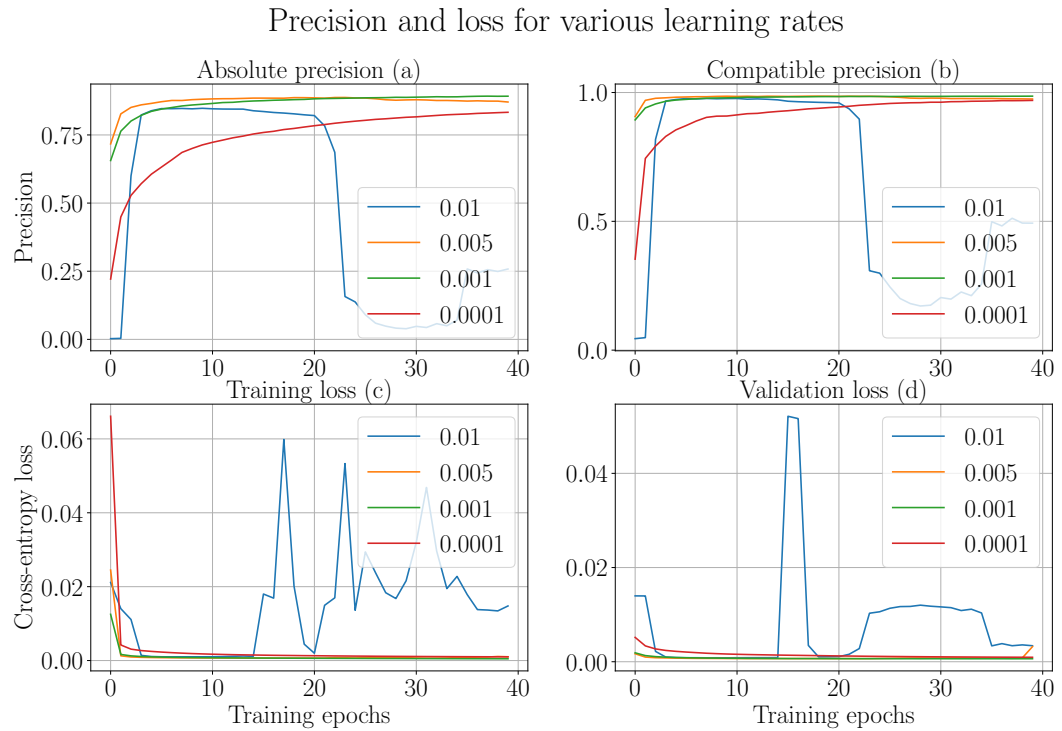
Figure 39.: **Performance of multiple learning rates**: The plot shows the performance of different values of learning rate. The subplots (a) and (b) show precision while (c) and (d) show the cross-entropy loss change over multiple epochs of training. High learning rates do not provide stable learning while a small one slows down the learning.

11.3.3. Activation

Many activation functions are used to find the best. Activations like *tanh*, *sigmoid*, *relu* and *elu* are utilised. Figure 40 shows the performances of these different activation functions. The activation functions *tanh*, *relu* and *elu* perform better than *sigmoid* on both the metrics, precision and loss. The activation functions *relu* and *elu* perform close to each other for precision as well as loss.
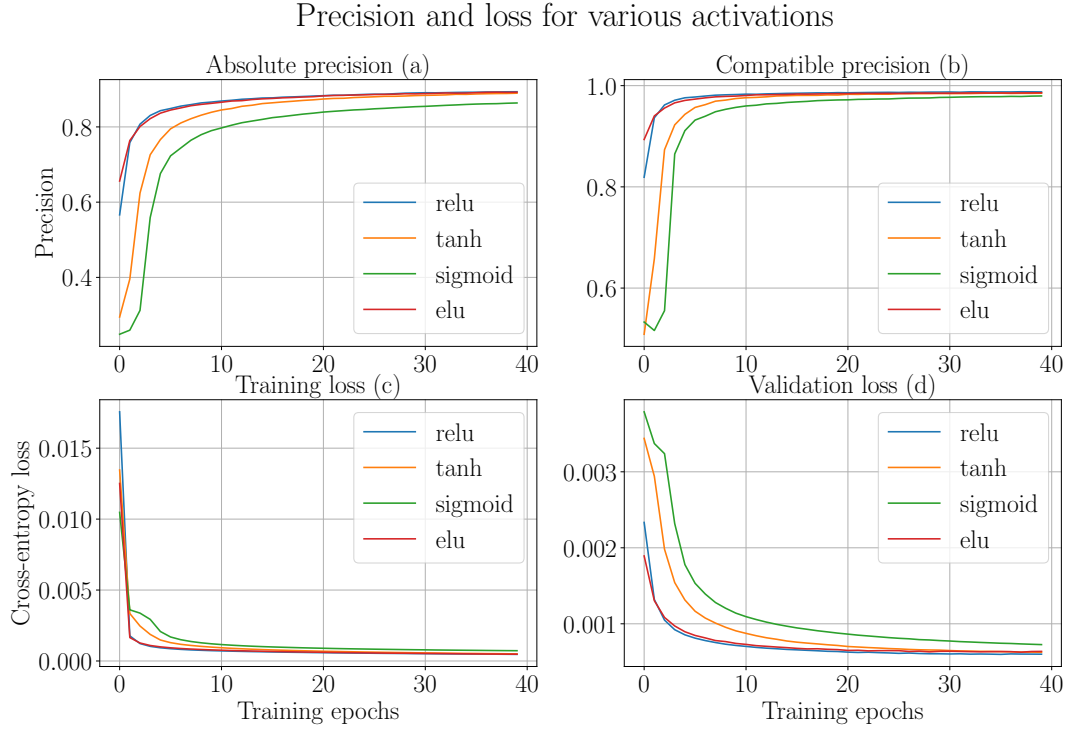
Precision and loss for various activations

Figure 40.: Performance of multiple activation functions: The plot shows the performance of different activation functions. The subplots (a) and (b) show the precision while (c) and (d) show cross-entropy loss change over multiple epochs of training.

11.3.4. Batch size

Many batch sizes are used to ascertain which one works to provide a stable learning. Different numbers like 64, 128, 256 and 512 are used as the mini-batch size. In mini-batch optimisation, a set of paths of size equal to the mini-batch size is taken and an average update is computed using these paths. This average update approximates the update for the whole set of paths. A smaller number would add more noise to the update because a smaller set would capture less variance of the complete set. The performance on various batch sizes is shown in figure 41. It is deduced from the plot that the batch size 64 is not performing well. In figure 41c, the training loss starts increasing instead of decreasing. This proves that 64 is not the right choice of the batch size. As batch size is increased, the precision improves and the loss drops. The drop is higher for a batch size 512 for the validation loss compared to the training loss. The baseline network uses 512 as batch size but another batch size 256 looks more promising and should be used.
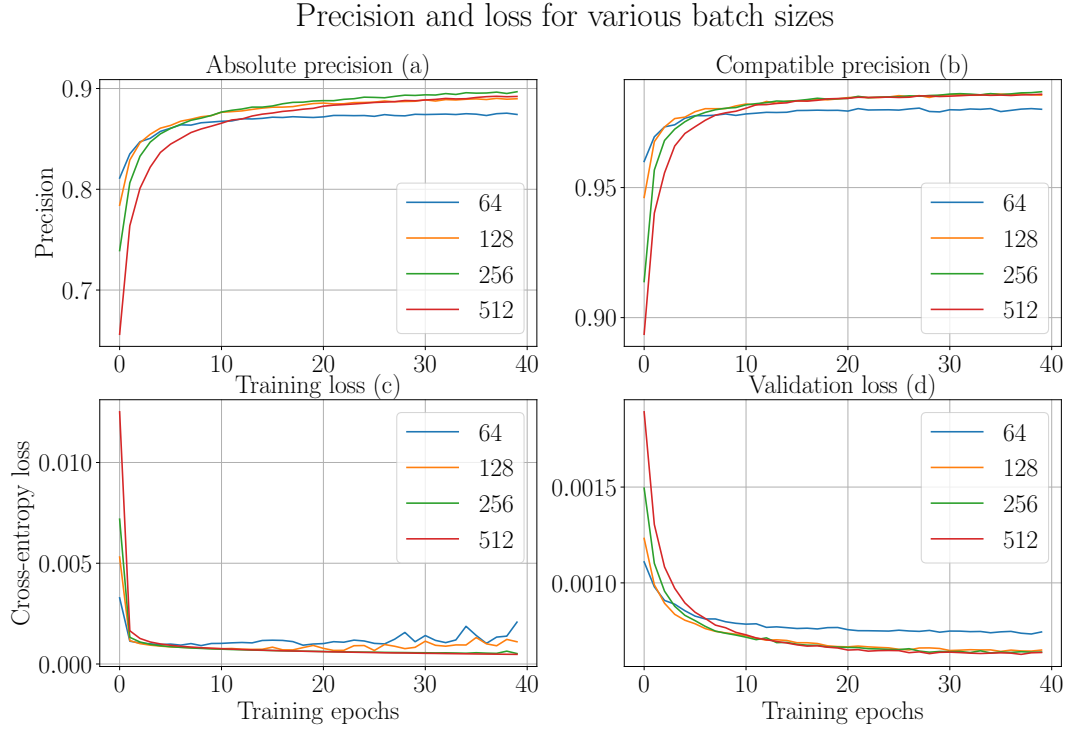
Precision and loss for various batch sizes

Figure 41.: Performance of different batch sizes: The plot shows the performance of different batch sizes. The subplots (a) and (b) show precision while (c) and (d) show the cross-entropy loss change over multiple epochs of training. The batch size 64 does not perform well compared to the larger batch sizes.

11.3.5. Number of recurrent units

Four different numbers for the recurrent units are used to see which one achieves the best performance. This number specifies the dimensionality of the hidden state. Higher the number, more expressive the model becomes. It means that the model's prediction strength or the "memory" of the model increases. This behaviour can be seen in figure 42. As the number of units increases, the precision becomes better and the loss drop is more. 512 number of units performs the best out of the four choices taken. But, the increasingly strong model tends to overfit and tries to memorise training paths. Combating overfitting is necessary when the network becomes strong. Using a higher number of memory units also increases the training time. With 64 as the number of memory units, the training time for each epoch was ≈ 6 minutes while with 512 memory units, each epoch took ≈ 45 minutes.
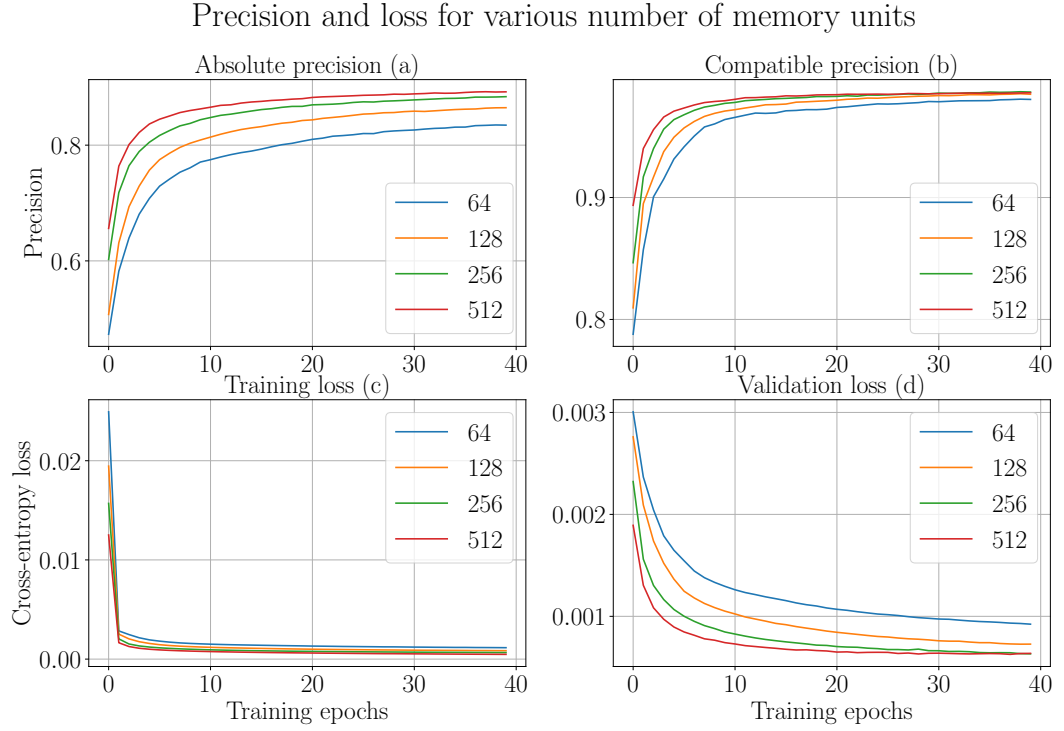
Figure 42.: Performance of multiple values of memory units: The plot shows the performance of different memory units. The subplots (a) and (b) show precision while (c) and (d) show the cross-entropy loss change over multiple epochs of training. 64 memory units for each recurrent layer do not perform well compared to the larger number like 256 or 512. The training time increases with the number of memory units.

11.3.6. Dropout

Dropout is used as a measure to overcome overfitting. To improve learning, the recurrent neural network is made stronger by adding more number of memory units and two hidden recurrent layers. Five different values of dropout are used to verify which one combats overfitting while keeping the performance high on unseen paths. Figure 43 shows the performance of different values of dropout. When no dropout (0.0) or smaller dropout (0.1) are used, the validation loss starts increasing while training loss still decreases. The precision starts decreasing for these values of dropout. It is a clear sign of overfitting. When a higher value (0.4) is used, the recurrent neural network becomes weaker and due to this, the precision increases slowly. 0.2 and 0.3 give better choices of dropout as they achieve better precision and the drop in the training and validation losses are more robust. The baseline

network configuration uses 0.2 as a dropout. A dropout 0.3 performs close to 0.2 and can be used as well. Higher the value of dropout, larger is the training time. Using no dropout approach took ≈ 33 minutes for training one epoch while with 0.4 dropout, it took ≈ 37 minutes [40].
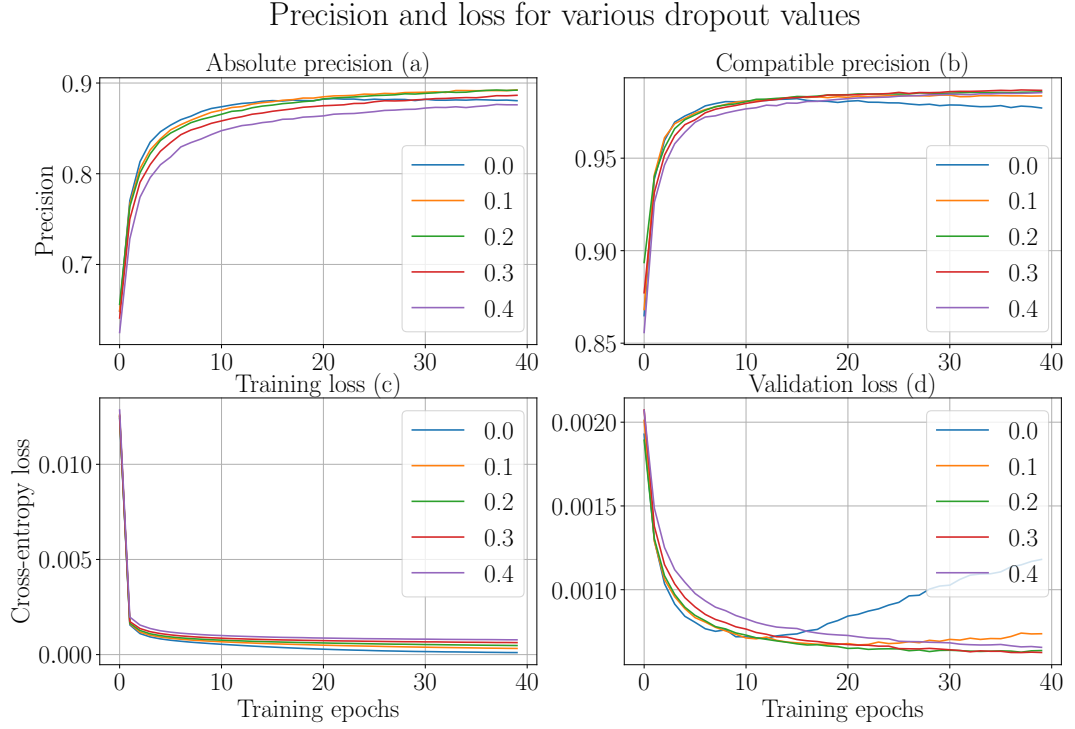
Figure 43.: **Performance of multiple values of dropout**: The plot shows the performance of different values of dropout. The subplots (a) and (b) show precision while (c) and (d) show the cross-entropy loss change over multiple epochs of training. No dropout shows overfitting as the validation loss increases during training (d) while a higher dropout (0.4) achieves lower precision.

11.3.7. Dimension of embedding layer

Embedding layer learns a fixed-length, unique dense vector for each tool. Larger the size of this layer, higher is its expressive power to distinguish among tools. But, with higher dimensions, there is a risk of overfitting and with a smaller dimension, underfitting can occur. Figure 44 shows the performance with different sizes of the embedding layer. All these sizes perform close to one another. The larger size performs slightly better than the lower size. The size $1,024$ performs the best while

64 also performs close especially for the training loss (figure 44c). The training time increased with the size of the embedding layer. For the size 64, it took ≈ 30 minutes for the training of one epoch while with $1,024$, it took ≈ 45 minutes.

Precision and loss for various sizes of embedding layer
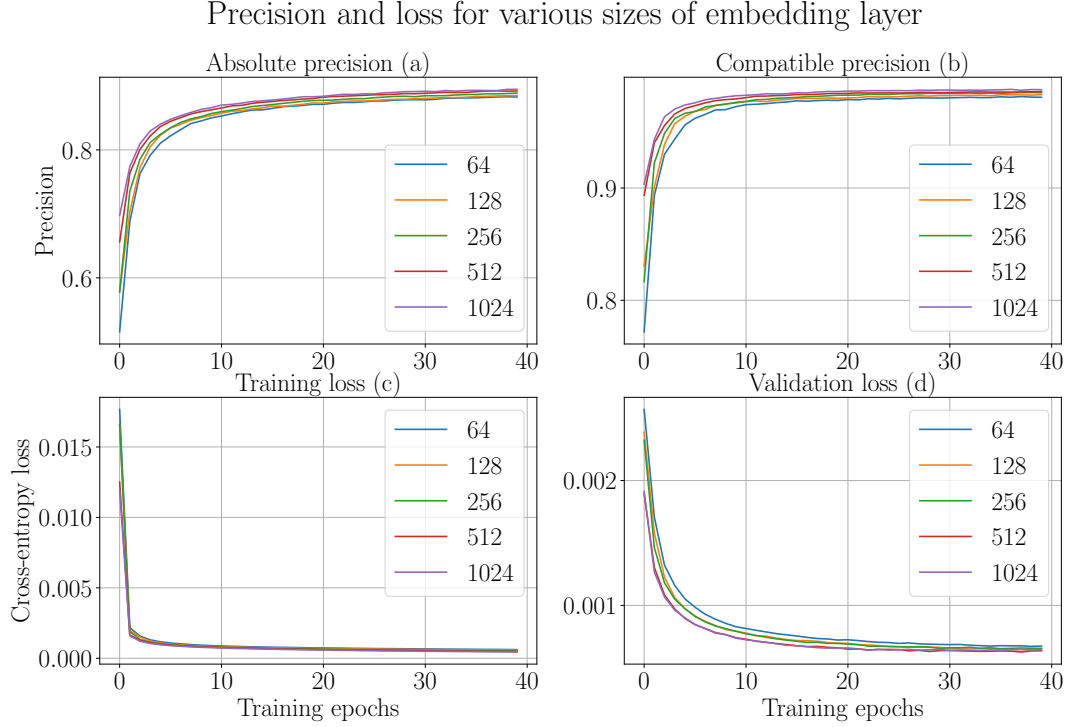

Figure 44.: Performance of different dimensions of embedding layer: The plot shows the performance of different dimensions of embedding layer. The subplots (a) and (b) show precision while (c) and (d) show the cross-entropy loss change over multiple epochs of training.

11.3.8. Accuracy (top-1 and top-2)

Absolute and compatible top-k accuracies are computed for training and test paths (figure 45). k is an integer and satisfies $k \geq 1$. All predicted next tools are sorted in descending order of their scores and then, top-k tools are extracted. The absolute top-k accuracy computes how many of the k predicted next tools are present in the set of actual next tools of a path. Top-1 (absolute and compatible) and top-2 (absolute and compatible) accuracies are computed. They are averaged for the training and test paths. For example, the absolute top-2 accuracy shows that how many of the two predicted next tools are present in the set of actual next tools of a path. An average of the absolute top-2 accuracy is computed for the training and test paths.

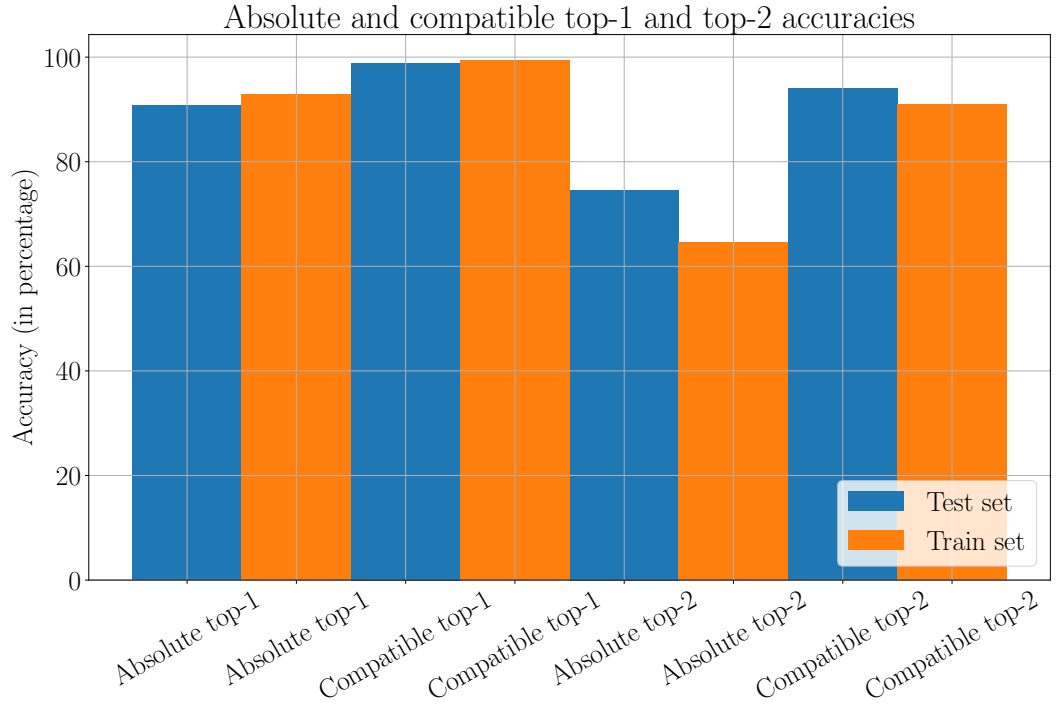A similar approach is followed for computing compatible top-k accuracy.

Figure 45.: Absolute and compatible top-1 and top-2 accuracies: The bar plot shows the absolute and compatible top-1 and top-2 accuracies. It also shows that the training and test paths achieve comparable performance.

Figure 45 shows that the performances of training and test paths remain similar for the absolute and compatible top-1 and top-2 accuracies. To compute absolute top-1 accuracy for a path, next tool with the highest score is selected and checked whether it is present in the set of actual next tools. This accuracy is averaged for all the paths. To compute compatible top-1, next tool with the highest score is checked if it is present in the set of compatible next tools (of the last tool of a path). The accuracies of compatible top-1 and top-2 are higher than that of the absolute top-1 and top-2 respectively. It shows that the recurrent neural network learns tool connections from multiple paths and use them in prediction. Top-1 achieves higher accuracy than top-2. There is a severe drop in the accuracy of absolute top-2 for the training and test paths. It is because many paths have just one next tool (actual next tool) in workflows. The compatible top-1 and top-2 accuracies remain high ($\geq 90\%$) for the training and test paths.

11.3.9. Precision with length of path

The variation of precision (absolute and compatible) with the length of paths is computed. The precision of predicting next tools for paths containing the same number of tools is averaged. This is done for the training and test paths. Figure 46 shows this variation.
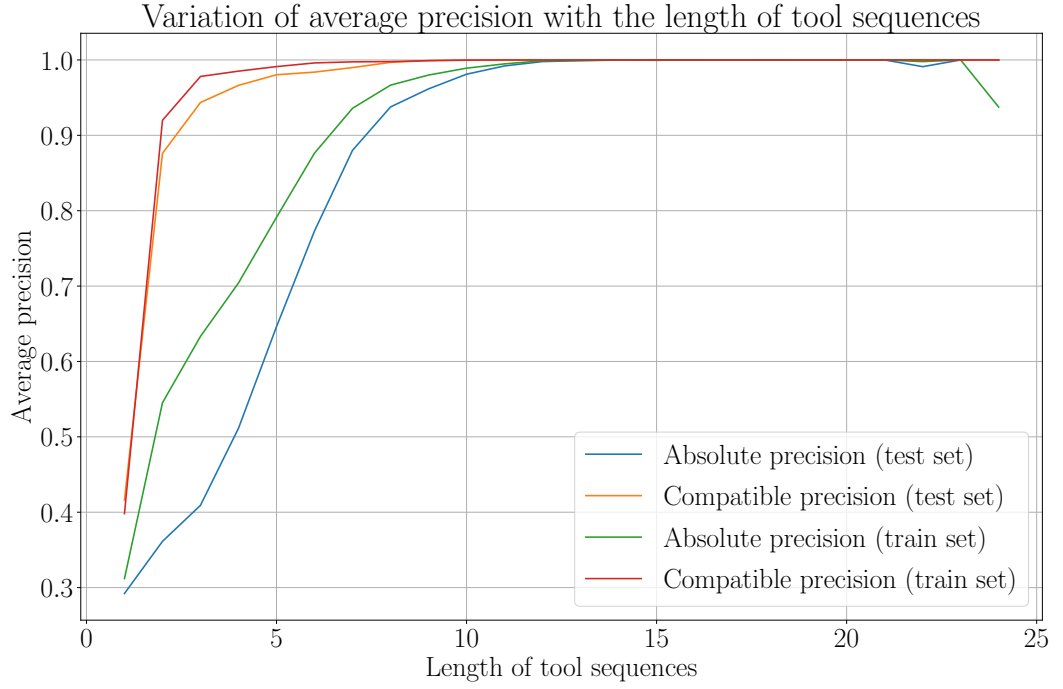
Figure 46.: Variation of precision with the length of paths: The plot shows how the length of path affects precision. It shows that as the length of paths increases, the precision becomes better. This improvement is more dominant for the compatible precision compared to the absolute precision.

As the maximum length of a path is fixed to 25, the plot shows maximum length as 24. The last tool is used as the next tool. It is concluded from the plot (figure 46) that as the length of paths increases, the precision becomes better. This increase is more dominant for the compatible precision compared to the absolute precision. As the length of paths increases, they have more tool connections and thereby more features. A higher number of features present in longer paths helps in predicting next tools more robustly. This is achieved even though the number of paths with lengths ≥ 20 is lower compared to the number of paths with shorter lengths.

11.3.10. Neural network with dense layers

A neural network with only dense layers is used as a classifier to compare the performance of learning on sequential data with recurrent neural network. Two hidden layers are used with 128 neurons each. The first layer is an embedding layer and the last (output) layer is a dense layer. The dropout (0.05) is applied to combat overfitting. Rest all the parameters remain the same as for the recurrent neural network. The training and test paths are decomposed in the same way as explained in section 11.2.3. The network is trained for 40 epochs. The precision (absolute and compatible) is computed after each training epoch. The training and validation losses are also noted. Figure 47 shows the performance of this network.

Precision and loss decomposing train and test paths (neural network with dense layers)
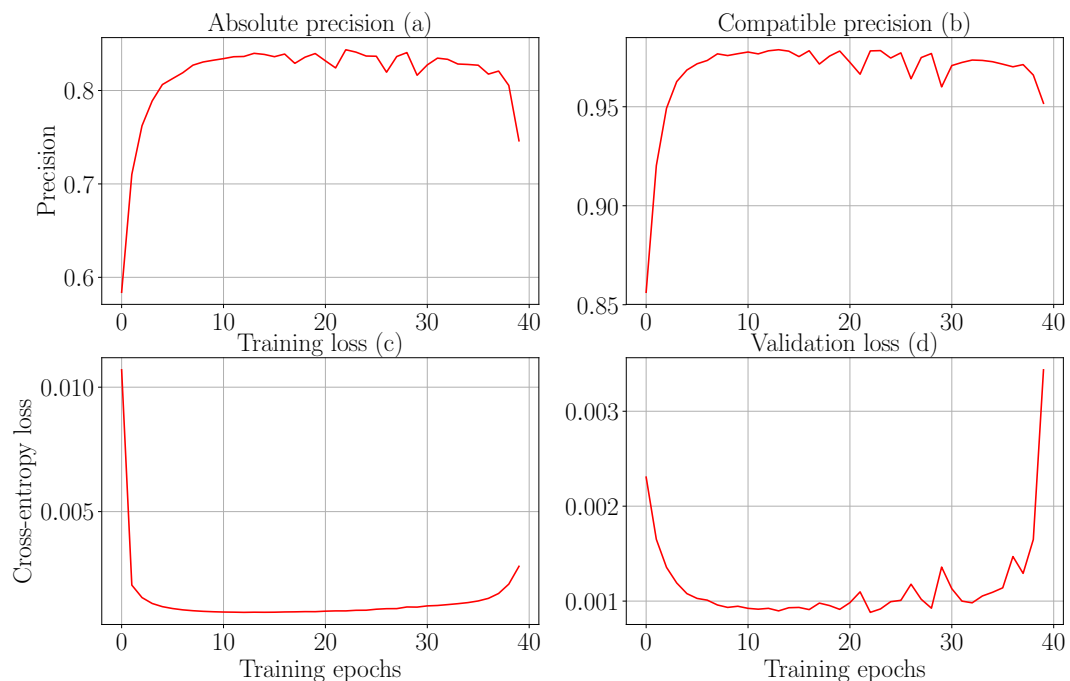
Figure 47.: Performance of a neural network with dense layers: The plot shows the performance of a neural network with dense layers. The paths are decomposed keeping the first tool fixed (as described in section 11.2.3). The subplots 47a and 47b show the absolute and compatible precision respectively. The subplots 47c and 47d show the training and validation losses respectively.

Figure 47a and 47b suggest that this network with dense layers also starts performing well (earlier in the epochs). It reaches an absolute precision of $\approx 83\%$ and

compatible precision of $\approx 97\%$ around the 15th epoch. The learning seems to be good in the beginning, but it starts becoming worse towards the end of training. The precision starts becoming worse. Moreover, the training and validation losses (figure 47c and 47d) start increasing. They collectively suggest that the network is overfitting. The neural network with recurrent layers performs better than this neural network with dense layers. It is concluded that the neural networks with recurrent layers are more suited for learning on sequential data than the neural networks with only dense layers.

12. Conclusion

The aim of the work was to predict next tools for paths (tool sequence). The workflows were first divided into paths and these paths were treated as sequential data. The paths in a workflow were considered independent. The recurrent neural network was used as a classifier to learn tools connections from these paths.

12.1. Network configuration

Many different configurations of the recurrent network were used to achieve higher precision without overfitting. Applying dropout was found to be beneficial to reduce overfitting. A larger number of memory units and larger size of embedding layer and mini-batch improved the precision. The optimisers with adaptive strategies performed well compared to the non-adaptive ones. A comparison was done to ascertain the best learning rate and activation.

12.2. The amount of data

A large number of workflows played a significant factor to improve precision. With a large number of workflow, it was ensured that the number of paths increased for each feature. Moreover, a more complex network with 512 memory units and 512 dimensional embedding layer could be used without overfitting. Collectively, they ensured higher precision. But, with an increased number of workflows and more complex network, the running time of the analysis also increased.

12.3. Decomposition of paths

For the idea of decomposing only test paths, the recurrent neural network was trained on longer paths. It failed to learn the semantics of smaller paths (present in test

paths). But, for the other ideas, where the training and test paths were decomposed identically, it performed well achieving $\approx 90\%$ absolute precision.

12.4. Classification

There were multiple tools as next tools for some paths. Therefore, multilabel classification approach was required. Compatible precision was higher than absolute precision for all the approaches of path decomposition. It may be because only the knowledge of next tools present in the training paths was used for prediction. Therefore, the predicted next tools did not match the actual next tools for some paths.

13. Future work

13.1. Use convolution

The recurrent neural network achieved a precision of $\approx 90\%$. Using convolutional layers along with the recurrent layers, the classification performance can be improved. The convolutional layers can be stacked above the recurrent layers to learn sub-features from the smaller parts of tool sequences. Convolution is well-suited to learn features irrespective of their positions.

13.2. Train on long paths and test on smaller

A poor performance was noted for the idea of decomposing only test paths. The detailed reasons should be found out and corrected to achieve a good precision for this approach. Different configurations of the recurrent neural network can be used to check whether they can improve the precision.

13.3. Restore original distribution

While taking unique paths into training and test sets, the original distribution of paths was not taken into consideration. The original distribution of paths should be restored for training paths only. Then, the recurrent neural network would assume that a path that repeats many times is more important.

13.4. Use other classifiers

The recurrent neural network was used as a classifier for this approach. *Bayesian network* and *markov fields* can be used as the classifiers to predict next tools. They may provide different insights. Multiple configurations of a neural network with dense layers can be researched to improve precision.

13.5. Decay prediction based on time

The tools which are deprecated and are not used anymore in Galaxy should be excluded from the analysis. To achieve that, the following two ideas can be used:

- Exclude the tools which are not used for a certain amount of time while processing the workflows. This should be done at the beginning of the analysis.

- Keep last used information for each tool. Remove those tools which are not being used anymore (deprecated) from the predictions. This should be done at the end.

Bibliography

[1] E. Afgan, D. Baker, M. Van Den Beek, D. Blankenberg, D. Bouvier, M. Cech, J. Chilton, D. Clements, N. Coraor, C. Eberhard, B. Grüning, A. Guerler, J. Hillman-Jackson, G. Von Kuster, E. Rasche, N. Soranzo, N. Turaga, J. Taylor, A. Nekrutenko, and J. Goecks, "The Galaxy platform for accessible, reproducible and collaborative biomedical analyses: 2016 update," *Nucleic Acids Research*, vol. 44, pp. W3–W10, July 2016.

[2] S. Robertson and H. Zaragoza, "The probabilistic relevance framework: Bm25 and beyond," *Found. Trends Inf. Retr.*, vol. 3, pp. 333–389, Apr. 2009.

[3] C. E. Shannon, "A mathematical theory of communication," *SIGMOBILE Mob. Comput. Commun. Rev.*, vol. 5, pp. 3–55, Jan. 2001.

[4] P. W. Foltz, "Latent semantic analysis for text-based research," *Behavior Research Methods, Instruments, & Computers*, vol. 28, pp. 197–202, Jun 1996.

[5] A. M. Shapiro and D. S. McNamara, "The use of latent semantic analysis as a tool for the quantitative assessment of understanding and knowledge," *Journal of Educational Computing Research*, vol. 22, no. 1, pp. 1–36, 2000.

[6] T. K. Landauer, "Learning and representing verbal meaning: The latent semantic analysis theory," *Current Directions in Psychological Science*, vol. 7, no. 5, pp. 161–164, 1998.

[7] J. Yang, "Notes on low-rank matrix factorization," *CoRR*, vol. abs/1507.00333, 2015.

[8] G. Shabat, Y. Shmueli, and A. Averbuch, "Missing entries matrix approximation and completion," vol. abs/1302.6768, 2013.

[9] Q. V. Le and T. Mikolov, "Distributed representations of sentences and documents," *CoRR*, vol. abs/1405.4053, 2014.

[10] G. I. Ivchenko and S. A. Honov, "On the jaccard similarity test," *Journal of Mathematical Sciences*, vol. 88, pp. 789–794, Mar 1998.

[11] S. Ruder, "An overview of gradient descent optimization algorithms," *CoRR*, vol. abs/1609.04747, 2016.

[12] I. Sutskever, J. Martens, G. Dahl, and G. Hinton, "On the importance of initialization and momentum in deep learning," pp. III–1139–III–1147, 2013.

[13] A. Botev, G. Lever, and D. Barber, "Nesterov's accelerated gradient and momentum as approximations to regularised update descent," pp. pp. 1899–1903., 2017.

[14] W. Yin, K. Kann, M. Yu, and H. Schütze, "Comparative study of CNN and RNN for natural language processing," *CoRR*, vol. abs/1702.01923, 2017.

[15] X. Li, T. Qin, J. Yang, and T. Liu, "Lightrnn: Memory and computation-efficient recurrent neural networks," *CoRR*, vol. abs/1610.09893, 2016.

[16] Z. C. Lipton, D. C. Kale, C. Elkan, and R. C. Wetzel, "Learning to diagnose with LSTM recurrent neural networks," *CoRR*, vol. abs/1511.03677, 2015.

[17] J. Chung, Ç. Gülçehre, K. Cho, and Y. Bengio, "Empirical evaluation of gated recurrent neural networks on sequence modeling," *CoRR*, vol. abs/1412.3555, 2014.

[18] N. Boulanger-Lewandowski, Y. Bengio, and P. Vincent, "Modeling temporal dependencies in high-dimensional sequences: Application to polyphonic music generation and transcription," 2012.

[19] A. McCarthy and C. K. Williams, "Predicting patient state-of-health using sliding window and recurrent classifiers," 2016.

[20] H. Jia, "Investigation into the effectiveness of long short term memory networks for stock price prediction," *CoRR*, vol. abs/1603.07893, 2016.

[21] F. J. Ordóñez and D. Roggen, "Deep convolutional and lstm recurrent neural networks for multimodal wearable activity recognition," *Sensors*, vol. 16, no. 1, 2016.

[22] S. Karan and J. Zola, "Exact structure learning of bayesian networks by optimal path extension," *CoRR*, vol. abs/1608.02682, 2016.

[23] P. Spirtes, C. Glymour, R. Scheines, S. Kauffman, V. Aimale, and F. Wimberly, "Constructing bayesian network models of gene expression networks from microarray data," 02 2002.

[24] D. M. Chickering, D. Heckerman, C. Meek, and D. Madigan, "Learning bayesian networks is np-hard," tech. rep., 1994.

[25] G. F. Cooper, "The computational complexity of probabilistic inference using bayesian belief networks (research note)," *Artif. Intell.*, vol. 42, pp. 393–405, Mar. 1990.

[26] D. M. Chickering, D. Heckerman, and C. Meek, "Large-sample learning of bayesian networks is np-hard," *J. Mach. Learn. Res.*, vol. 5, pp. 1287–1330, Dec. 2004.

[27] A. Sarkar and D. B. Dunson, "Bayesian nonparametric modeling of higher order markov chains," vol. abs/1506.06268, 2015.

[28] K. Cho, B. van Merrienboer, D. Bahdanau, and Y. Bengio, "On the properties of neural machine translation: Encoder-decoder approaches," *CoRR*, vol. abs/1409.1259, 2014.

[29] R. Pascanu, T. Mikolov, and Y. Bengio, "Understanding the exploding gradient problem," *CoRR*, vol. abs/1211.5063, 2012.

[30] S. Hochreiter and J. Schmidhuber, "Long short-term memory," *Neural Comput.*, vol. 9, pp. 1735–1780, Nov. 1997.

[31] M. Hermans and B. Schrauwen, "Training and analysing deep recurrent neural networks," pp. 190–198, 2013.

[32] D. Clevert, T. Unterthiner, and S. Hochreiter, "Fast and accurate deep network learning by exponential linear units (elus)," *CoRR*, vol. abs/1511.07289, 2015.

[33] N. Srivastava, G. Hinton, A. Krizhevsky, I. Sutskever, and R. Salakhutdinov, "Dropout: A simple way to prevent neural networks from overfitting," *Journal of Machine Learning Research*, vol. 15, pp. 1929–1958, 2014.

[34] W. Zaremba, I. Sutskever, and O. Vinyals, "Recurrent neural network regularization," *CoRR*, vol. abs/1409.2329, 2014.

[35] Y. Gal and Z. Ghahramani, "A theoretically grounded application of dropout in recurrent neural networks," pp. 1027–1035, 2016.

[36] S. Ruder, "An overview of gradient descent optimization algorithms," *CoRR*, vol. abs/1609.04747, 2016.

[37] M. Li, T. Zhang, Y. Chen, and A. J. Smola, "Efficient mini-batch training for stochastic optimization," in *Proceedings of the 20th ACM SIGKDD International Conference on Knowledge Discovery and Data Mining*, KDD '14, (New York, NY, USA), pp. 661–670, ACM, 2014.

[38] D. P. Kingma and J. Ba, "Adam: A method for stochastic optimization," *CoRR*, vol. abs/1412.6980, 2014.

[39] A. Graves, "Generating sequences with recurrent neural networks," *CoRR*, vol. abs/1308.0850, 2013.

[40] S. Wang and C. Manning, "Fast dropout training," vol. 28, pp. 118–126, 17–19 Jun 2013.

A. Appendix

A.1. Visualisers

To showcase similar tools, the visualisers are created. For the *latent semantic analysis* approach, there are two websites and for the paragraph vectors approach, there is one. In addition to showing similar tools for the selected tool, they show a few plots for the error, gradient, learning rates and the selected tool's similarity scores with all the other similar tools.

- Use full-rank document-token matrices[1].

- Use 5% of full-rank document-token matrices[2].

- Paragraph vectors[3]

A.2. Code repositories

The following sections provide the location of the codebase (*github* repositories) used for this work. All the repositories are under MIT license.

A.2.1. Find similar scientific tools

There are separate branches for the different approaches (*latent semantic analysis* and *paragraph vectors*). For *latent semantic analysis* approach, there are two branches:

- Full-rank document-token matrices[4].

---

[1]https://rawgit.com/anuprulez/similar_galaxy_tools/lsi/viz/similarity_viz.html
[2]https://rawgit.com/anuprulez/similar_galaxy_tools/lsi_005/viz/similarity_viz.html
[3]https://rawgit.com/anuprulez/similar_galaxy_tools/doc2vec/viz/similarity_viz.html
[4]https://github.com/anuprulez/similar_galaxy_tools/tree/lsi

- Document-token matrices reduced to 5% of the full-rank[5].

Both these branches differ only in their ranks of corresponding document-token matrices. There is a separate branch for *paragraph vectors* approach[6].

A.2.2. Predict next tools in scientific workflows

The Galaxy workflows are represented as the directed acyclic graphs and they can be visualised in a website[7]. The workflow chosen from the dropdown is displayed as a cytoscape[8] graph. The separate code repositories are maintained for the ideas discussed in section 9.5.1. They are listed as follows:

- No decomposition of paths[9]

- Decomposition of only test set[10]

- Decomposition of test and train sets[11]

---

[5]`https://github.com/anuprulez/similar_galaxy_tools/tree/lsi_005`
[6]`https://github.com/anuprulez/similar_galaxy_tools/tree/doc2vec`
[7]`https://rawgit.com/anuprulez/similar_galaxy_workflow/master/viz/index.html`
[8]`http://js.cytoscape.org/`
[9]`https://github.com/anuprulez/similar_galaxy_workflow/tree/train_longer_paths`
[10]`https://github.com/anuprulez/similar_galaxy_workflow/tree/train_long_test_decomposed`
[11]`https://github.com/anuprulez/similar_galaxy_workflow/tree/extreme_paths`